Simplify your imaging workflows

Make research imaging workflows accessible, traceable, and secure with Athena Software for Core Imaging Facilities.

Thermo Scientific™ Athena Software is a premium imaging data management platform designed for core imaging facilities that support materials science research.

Athena Software ensures traceability of images, metadata, and experimental workflows through an intuitive and collaborative web interface.

Find out more at **thermofisher.com/athena**

ThermoFisher SCIENTIFIC

ADVANCED OPTICAL MATERIALS
www.advopticalmat.de

Carbon Dots for Photocatalytic Degradation of Aqueous Pollutants: Recent Advancements

Kamran Akbar, Elisa Moretti,* and Alberto Vomiero**

The immense progress of humanity on the technological, domestic, and industrial fronts comes at the cost of polluting the planet. Aquatic pollution is particularly dangerous since all life forms are directly linked to it. Each year tons of industrial and domestic pollutants make their way into aqueous systems. Efficient removal/degradation of these pollutants is of prime importance for the sustainable future. Among many technologies, photodegradation is an emerging and promising method for the successful removal of aqueous pollutants since it is powered by abundant solar light. The last decade had shown that carbon dots are among the most promising materials that can be utilized as an efficient tool to derive various solar-driven chemical reactions. Carbon dots possess unique photophysical and chemical properties such as light-harvesting over a broad-spectrum region, upconversion photoluminescence, photosensitizers, chemical inertness, and bivalent redox character, etc. The ease of synthesis of carbon dots at low cost also contributes hugely to their utilizations as an efficient photocatalyst for the degradation of aqueous pollutants. This review summarizes the recent progress made in the field of photodegradation of aqueous pollutants with the aid of carbon dots and their hybrids, highlighting the critical role carbon dots can play in the field.

1. Introduction

Carbon dots (C-dots) are 0D quasi-spherical particles with a size of <10 nm and were first discovered in 2004 during the purification of single-walled carbon nanotubes.[1] Chemically, C-dots are composed of sp^2/sp^3 hybridized carbon atoms.[2] Compared to other allotropes of carbon, C-dots have unique photophysical and chemical properties such as light absorption over a wide range,[3,4] bright photoluminescence (PL),[5] electron mediation,[6,7] excellent photostability,[8] high aqueous solubility,[9] upconversion,[10,11] photosensitization,[12] chemical inertness,[13] facile functionalization,[14] and low toxicity due to their nonmetallic nature. In addition, a plethora of inexpensive precursors and a variety of approaches are available for their synthesis. All these features lead to their explosive utilization in distinct areas such as photocatalysis,[15,16] biomedical imaging,[17] sensors,[18] photovoltaic panels,[19,20] drug delivery,[21] and numerous other technologies.[22–24]

The structural core of carbon dots can be either amorphous, crystalline, or partially crystalline. Crystalline carbon dots are usually derived from graphene via top-down synthetic methods and are denoted as graphene quantum dots (GQDs).[25] However, there are multiple reports where carbon dots with crystalline graphitic core are obtained via bottom-up synthetic methods and subsequently referred to as GQDs.[26–28] On the contrary, other research groups preferred to call them carbon quantum dots (CQDs).[10,29,30] Further, the CQDs term is also interchangeably used for amorphous carbon dots. Other terms include carbon nanodots (CNDs) or simply carbon dots (CDs) for amorphous or partially crystalline structures.[31,32] For the sake of simplicity, in this review, we will stick with the term "C-dots" for all of the above-mentioned carbon dot structures with sizes in the range of <10 nm.

Tons of industrial and domestic pollutants are spilled each day into waterways, which are harmful not only to the environment and human health but also to natural echo systems.[32,33] Efficient and cost-effective removal of these pollutants is crucial for our sustainable future. Among many contenders, photocatalytic technologies stand out due to the utilization of semiconductors and inexpensive sunlight for the removal of these pollutants.[34] Most pollutants in waterways can either be small organic compounds such as dyes, drugs, or long-chain organic molecules such as perfluorooctanoic acid and perfluorooctane sulfonate, which are regarded as persistent organic pollutants. Other major category includes toxic metals such as Cd and Cr. Significant developments in the past decade now allow photodegradation of numerous of these pollutants via C-dots and

Dr. K. Akbar, Prof. E. Moretti, Prof. A. Vomiero
Department of Molecular Sciences and Nanosystems
Ca' Foscari University of Venice
Via Torino 155, Venezia Mestre 30172, Italy
E-mail: kamran.akbar@unive.it; elisa.moretti@unive.it;
alberto.vomiero@unive.it, alberto.vomiero@ltu.se

Prof. A. Vomiero
Division of Materials Science
Department of Engineering Sciences and Mathematics
Luleå University of Technology
Luleå 97187, Sweden

The ORCID identification number(s) for the author(s) of this article can be found under https://doi.org/10.1002/adom.202100532.

DOI: 10.1002/adom.202100532

their hybrids. Tunability in C-dots structure, low-cost synthesis, nonmetallic nature, excellent photophysical, and chemical properties make them a viable candidate for commercial utilization. In this review, we will focus on recent developments in the utilization of C-dots and their hybrids for the photodegradation of pollutants that make their way into aqueous systems. C-dots are capable of removing pollutants from aqueous solutions based on the adsorption phenomenon owing to their large surface area and the topic has been reviewed recently.[18,35] Further, we will not review recent developments on the synthesis of C-dots as it has already been covered in many recent reviews in detail.[36,37]

2. Photocatalytic Degradation

Photocatalytic degradation or simply photodegradation is a process in which ultraviolet (UV), visible (Vis), or infrared (IR) light is utilized to transform an environmental pollutant into a benign or less harmful product over a solid surface known as photocatalyst. In a light-absorbing event, a typical semiconductor photocatalyst absorbs the radiation which excites an electron (e^-) from its valence band (VB) to its conduction band (CB) leaving a hole (h^+) in VB (**Scheme 1**). Generated electrons and holes are photoreactive species and can drive the various redox reactions depending on the redox potential of the reaction and electronic band structure of the photocatalyst. Such redox reactions also include the conversion of dissolved oxygen and OH ions into their respective radicals. Transfer of electron (reduction) to molecular oxygen transforms it into reactive superoxide anion ($^{\bullet}O_2^-$), conversely transfer of hole (oxidation) to OH^- into reactive $^{\bullet}OH$ radical. These reactive radical species are capable of degrading organic pollutants via their conversion into harmless CO_2 and H_2O.[38] Thus, in the photodegradation process, light plays a role of a reagent that transforms an environmental pollutant into harmless or benign products. Rapid recombination of electron–hole pair without the formation of reactive radical species severally limits the photodegradation activity. Recombination can proceed via the emission of heat or radiation. When emission is in the form of radiation, it is known as photoluminescence. Numerous studies found that C-dots have excellent photoluminescence properties. Although photoluminescence has numerous applications such as biomedical imaging, it is a competing process during photodegradation. Similarly, the emission of heat is useful for photothermal applications but it will lead to reduced photodegradation efficiencies.

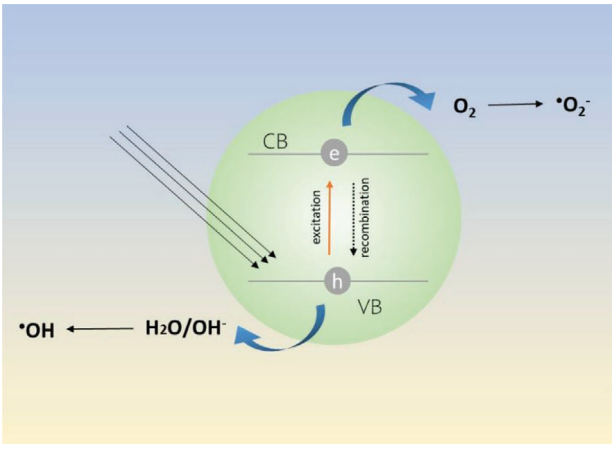

Scheme 1. A representation of the production of reactive radical species over a semiconductor under excitation from a light source in aqueous solutions.

3. Role of C-Dots in Photodegradation

The role of C-dots in photodegradation can be divided as 1) C-dots as photocatalysts, 2) C-dots as photosensitizers, 3) C-dots as electron acceptor/mediators, and 4) C-dots as up-conversion materials.

3.1. C-Dots as Photocatalysts

Photocatalysis is defined as "Change in the rate of a chemical reaction or its initiation under the action of ultraviolet, visible or infrared radiation in the presence of a substance (the photocatalyst) that absorbs light and is involved in the chemical transformation of the reaction partners."[39] Carbon dots can harvest light by direct absorption. The absorbed photons excite electrons from their highest occupied molecular orbital (HOMO) to their lowest unoccupied molecular orbital (LUMO) by leaving a hole in HOMO. Generated electrons and holes then result in chemical transformation of reaction partners rendering C-dots as photocatalysts.

C-dots have strong capabilities to absorb light in the UV-vis range due to π–π^* transition of sp^2 C=C double bonds present in the inner core (represented in **Figure 1**a as core state).[8,40,41] Outer layer of C-dots contains various functional groups (−COOH, −OH, $-NH_2$, etc.) depending on the synthetic route (represented in Figure 1a as a surface state). These functional groups also respond to excitation light sources and most often their absorption occurs in the Vis range due to n– π^* as shown in Figure 1. It is worth mentioning that C-dots are not unique in absorption in the UV–Vis range: other carbon allotropes such as graphene oxide, multilayer graphene, carbon nanotubes, etc. also show a similar absorption profile. This is perhaps because of similar underlying sp^2 C=C double bond structure present in these allotropes.[42] The benefits of C-dots come into play due to their ultrasmall size, aqueous solubility, and ease of their synthesis.

Although in literature, C-dots are also sometimes termed quantum dots, in most of the cases they hardly show any resemblances to typical semiconductor quantum dots, exhibiting strongly confined electronic quantum states. The absorption phenomenon in C-dots is different from typical semiconductor quantum dots, where the size of the quantum dot defines its bandgap and consequently its absorption/emission wavelength. The smaller the size, the greater is the bandgap due to quantum confinement. Evidence of true quantum confinement in C-dots is yet to be univocally demonstrated and the topic remains largely controversial. Earlier studies, designed to test the effect of size of C-dots on their absorption properties,

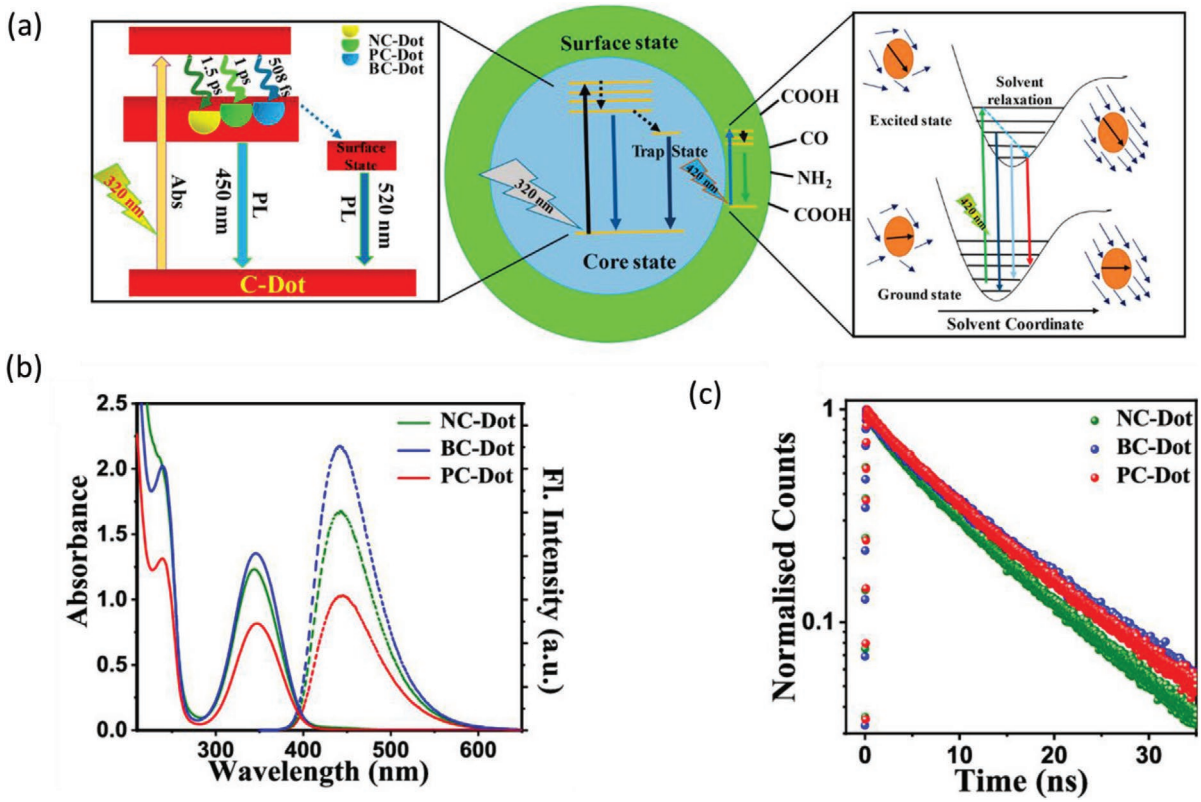

Figure 1. a) Schematic representation of excited-state processes for doped C-dots excited at core state (at 320 nm) and surface state (at 420 nm). b) Steady-state absorption (solid lines) and emission (dashed lines) spectra and c) time-resolved emission measurements ($\lambda_{ex} = 340$ nm, $\lambda_{em} = 450$ nm) of the doped C-dots. Reproduced with permission.[8] Copyright 2019, American Chemical Society.

concluded that expansion of sp^2 network within C-dots core (which would increase if the size of C-dot increased) has a more prominent effect on their absorption characteristics rather than expansion of actual physical dimensions of C-dots.[43,44]

Absorption in the UV range is however not as beneficial for most of the photocatalysis applications, as the majority of solar energy is concentrated in the Vis region. Near-infrared (NIR) or mid-infrared (MIR) is also useful as it would allow thermal radiation harvesting. Recently, several studies have demonstrated that the absorption of C-dots can be red-shifted to NIR-I regions via manipulations of surface functional groups. F.A. Permatasari et al. have shown that the addition of pyrrolic-nitrogen on the CD surface leads to a redshift in absorption from 550 to 650 nm as shown in **Figure 2**a.[45] These doped CDs showed a strong photothermal effect in an aqueous solution and can raise its temperature under laser excitation as shown in Figure 2b. Geng et al. showed that the introduction of graphitic nitrogen in C-dots leads to absorption in the NIR-II range (808 and 1064 nm) as shown in Figure 2c.[46] As a result, the photothermal conversion efficiency of 81.3% was achieved in the NIR-II window with a graphitic nitrogen content of 4.30%. Mechanistic studies to find the origin of NIR-II absorption in these CD are represented in Figure 2d–f. Authors argue that the electron paramagnetic resonance (EPR) signal of CD can be assigned to a singly occupied defect level (paramagnetic F center). Doped graphitic N atoms induce F color centers to mediate optical transitions from the HOMO level to singly occupied defect levels (F centers) and from F centers to the higher LUMO level under the NIR excitation. As a result, a photothermal efficiency of 4.3% was realized for doped samples. Further details regarding the effect of doping, particle size, surface functional group modifications on absorption/emission properties of C-dots can be found in an excellent review by Ding et al.[17]

Despite significant progress in the enhancement of absorption/emission properties C-dots, recent outcomes of several studies cast some doubts on actual progress made in the field. For instance, the separation of the highly fluorescent molecular fluorophore (**Figure 3**) from synthesized C-dots powders suggests that remarkable absorption and luminescence properties of C-dots do not solely originate from C-dots.[47] These molecular fluorophores can crystallize via similar drying processes adopted in most C-dot synthetic protocols.[48] Further, transmission electron microscopy and d-spacing (0.21 nm) data of these molecular fluorophores (Figure 3c) are identical to C-dots and graphitic core d-spacing calculations. In this perspective, excellent work from Baker's group should be taken as a guideline while dealing with C-dots (Figure 3b,d).[49] In this work, Baker et al. showed that wide-spread utilization of low molecular weight cutoff (MWCO) dialysis membranes (<20 kDa) do not assure efficient removal of the majority of highly fluorescent molecular species. Thus, appropriate purification methods are crucial owing to the ubiquitous formation of molecular fluorescent entities, especially via bottom-up synthetic protocols.

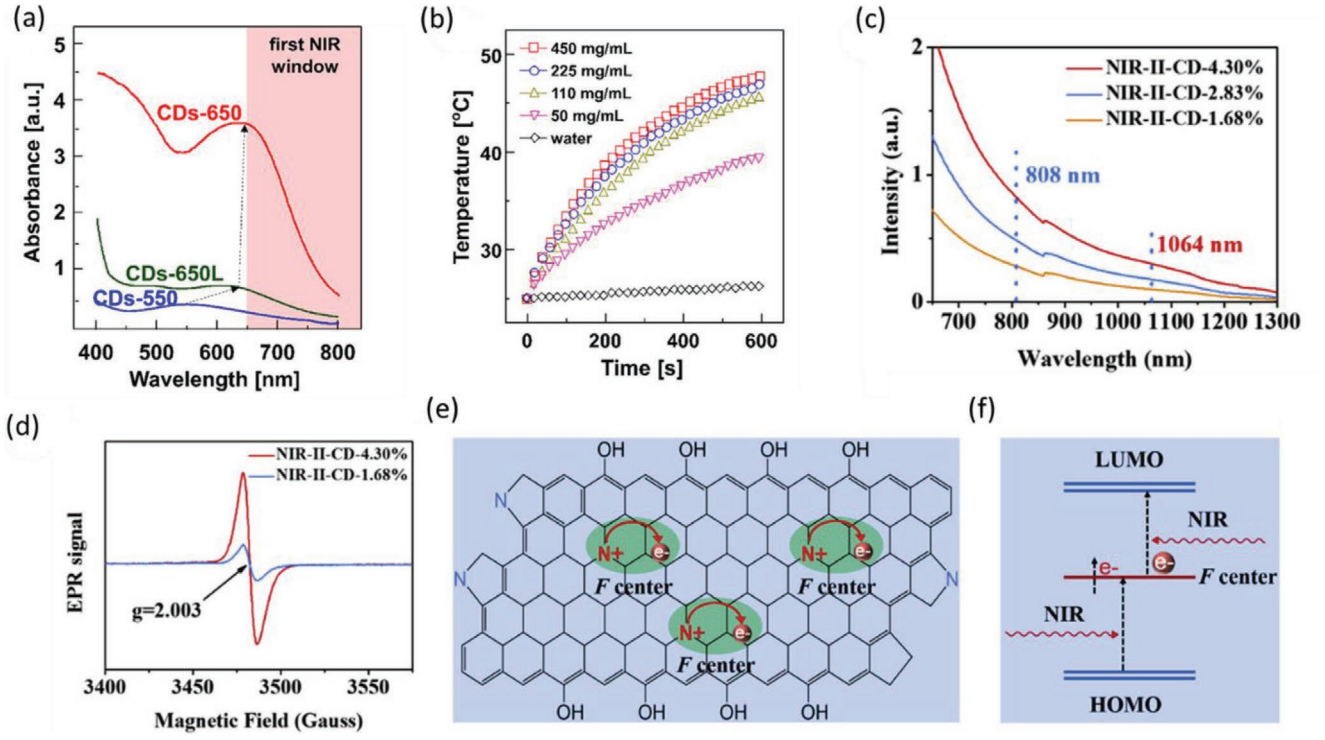

Figure 2. a) UV–vis absorption spectra of different nitrogen-doped C-dots. b) Photothermal performances of carbon dots in ultrapure water as indicated by temperature elevation as a function of laser irradiation time for 10 min. a,b) Reproduced with permission.[45] Copyright 2018, American Chemical Society. c) NIR absorption spectra of three NIR-II CD samples with different graphitic nitrogen content. d) EPR signals of NIR-II CD powders measured at room temperature. e) The proposed formation mechanism of F centers at graphitic N sites, where N atoms donate one excess electron and form N^+ cations to trap the electron with large binding energy. f) Defect energy levels of doped graphitic N as an F center within the wide bandgap of NIR-II-CDs and possible optical transitions from the HOMO level to the defect level and from the singly occupied defect level to the LUMO level under the NIR excitation. c–f) Reproduced with permission.[46] Copyright 2019, Elsevier.

3.2. Carbon Dots as Photosensitizer

Photosensitization is defined as "The process by which a photochemical or photophysical alteration occurs in one molecular entity as a result of initial absorption of radiation by another molecular entity called a photosensitizer. In mechanistic photochemistry, the term is limited to cases in which the photosensitizer is not consumed in the reaction."[39] Traditionally, aromatic hydrocarbons (with highly conjugated systems that promote electron delocalization) and organometallic complexes of electron-rich metals (such as iridium, ruthenium, and rhodium) are regarded as excellent photosensitizers. The common feature between the two is the fact that their electrons are easily excitable even at low energies and the presence of a large continuum of orbitals within both HOMO and LUMO. These orbitals allow excited electrons to switch multiplicities via intersystem crossing and prolong the lifetime of the excited state. This prolonged lifetime ultimately enriches the chance of the photosensitization process.[50,51] Because of these reasons, photosensitization is often an efficient way to induce a photochemical reaction even in the case of low absorption coefficient or when a competing process such as fluorescence takes place (which is most often the case with C-dots),[39] During the photosensitization process, a photosensitizer absorbs the light and move to an excited energy state. In the case of C-dots, this excited state is capable of transferring some of its excitation energy to an external entity such as adsorbed molecular oxygen. During this energy transfer process, molecular oxygen, which is usually present in triplet ground state ($^3O_2$) transforms into highly reactive singlet oxygen ($^1O_2$). Second, excited electrons in photosensitizer can also be transferred to adsorbed oxygen, converting it into reactive superoxide anion ($^{\bullet}O_2^-$). In this second case, the process of photosensitization is closely related to photocatalysis. Nevertheless, the production of singlet oxygen is exclusive to the process of photosensitization. Numerous studies have confirmed the role of carbon dots as photosensitizers due to the presence of highly delocalized electrons and additional energy levels between HOMO and LUMO. For instance, Wu et al. reported the production of both of these reactive oxygen species over nitrogen-doped C-dots as shown in **Figure 4**a.[52] The authors concluded that the presence of graphitic nitrogen in C-dots was responsible for triplet activation, while the presence of pyrrolic nitrogen was mainly responsible for the adsorption of oxygen on C-dots. Electron paramagnetic resonance (EPR) studies (Figure 4) with 2,2,6,6-tetramethylpiperidine (TEMP) and 5,5-dimethyl- 1-pyrroline-N-oxide (DMPO) confirms the production of $^1O_2$ and $^{\bullet}O_2^-$, respectively.

3.3. C-Dots as Electron Mediators

C-dots possess bivalent redox character, which means they can either act as electron acceptors or can donate their electrons upon photoexcitation, depending on their surface functionality

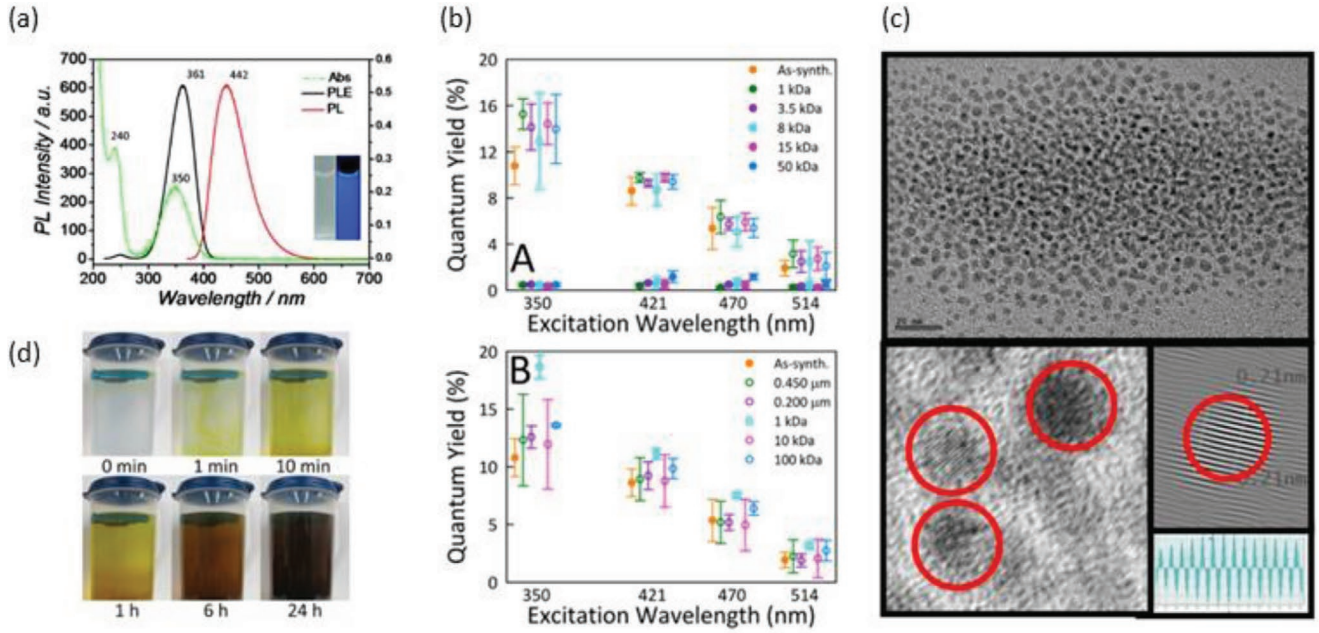

Figure 3. a) PL and absorbance spectra of fluorescent molecular fluorophore (imidazo [1,2-a]pyridine-7-carboxylic acid) obtained from as-synthesized CDs via chromatographic separation. Reproduced with permission.[47] Copyright 2019, Royal Society of Chemistry. b) Fluorescence quantum yields measured following (A) dialysis and (B) ultrafiltration cleanup of citric acid and urea-derived fluorescent carbon dots. The retentate results are represented by closed symbols, and dialysate/filtrate quantum yields are denoted by open symbols. These results show that in the as-synthesized samples, the majority of the fluorescence observed was due to smaller species permeating through membranes rather than retentates, which show much weaker fluorescence. Reproduced with permission.[49] Copyright 2018, American Chemical Society. c) Transmission electron microscopy image of methylene succinic acid separated molecular fluorophore obtained from fluorescent carbon dots, showing similar d-spacing as of graphitic carbon. Reproduced with permission.[48] Copyright 2017, Royal Society of Chemistry. d) Vivid progression of dialysis (with 1 kDa MWCO membrane) at various times. Reproduced with permission.[49] Copyright 2018, American Chemical Society.

and conjugation with other surfaces. For instance, Strauss et al. demonstrated that perylenediimides (which have a strong tendency to accept photogenerated electrons) can accept photogenerated electrons from CNDs upon photoexcitation.[53] On the other hand, molecules with electron-donating properties such as porphyrin can easily transfer their photogenerated electrons towards CNDs.[54] Electron acceptor properties of C-dots are due to the presence of extensively conjugated π-networks within their core.[55,56] Electron accepting properties specifically come in hand in conjunction with semiconductors, where efficient charge separation is needed.[57] C-dots can accept photogenerated electrons from a semiconductor during an excitation event, thus preventing generated electrons to recombine with holes, which ultimately leads to improved photocatalytic efficiency.[58]

Structural tuning via the addition of electron-acceptor and electron-donor group onto C-dots can further allow manipulation of their properties.[59] Srivastava et al. passivated the surface of C-dots with electron-acceptor and electron-donor groups (**Figure 5**) and tested their photophysical properties both in bulk state and at the single-particle level. Density functional theory (DFT) calculations and bulk state experiments reveal that this

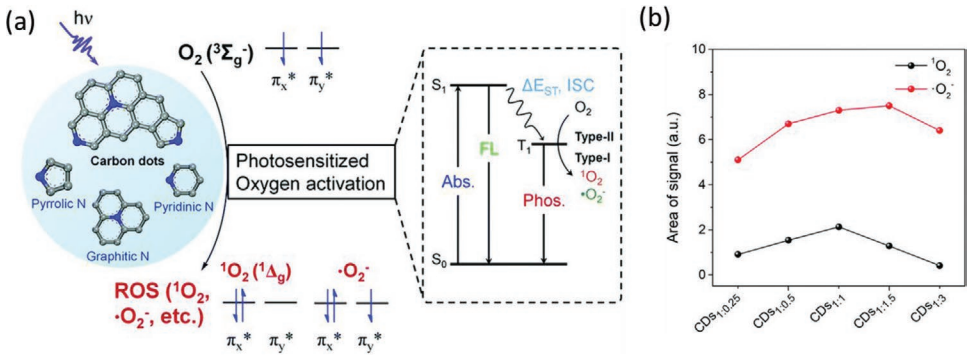

Figure 4. a) Effect of nitrogen doping on C-dots for production of reactive oxygen species (ROS) such as $^1O_2$ and $^\bullet O_2^-$ via photosensitization effect under UV-illumination. b) EPR integration intensities of $^1O_2$ and $^\bullet O_2^-$ with respect to the percentage increase of nitrogen content in C-dots. Nitrogen content was 5.4, 9.4, 10.7, 13.3, and 16.0% for $CDs_{1:0.25}$, $CDs_{1:0.5}$, $CDs_{1:1}$, $CDs_{1:1.5}$ and $CDs_{1:3}$ respectively. Reproduced with permission.[52] Copyright 2020, Royal Society of Chemistry.

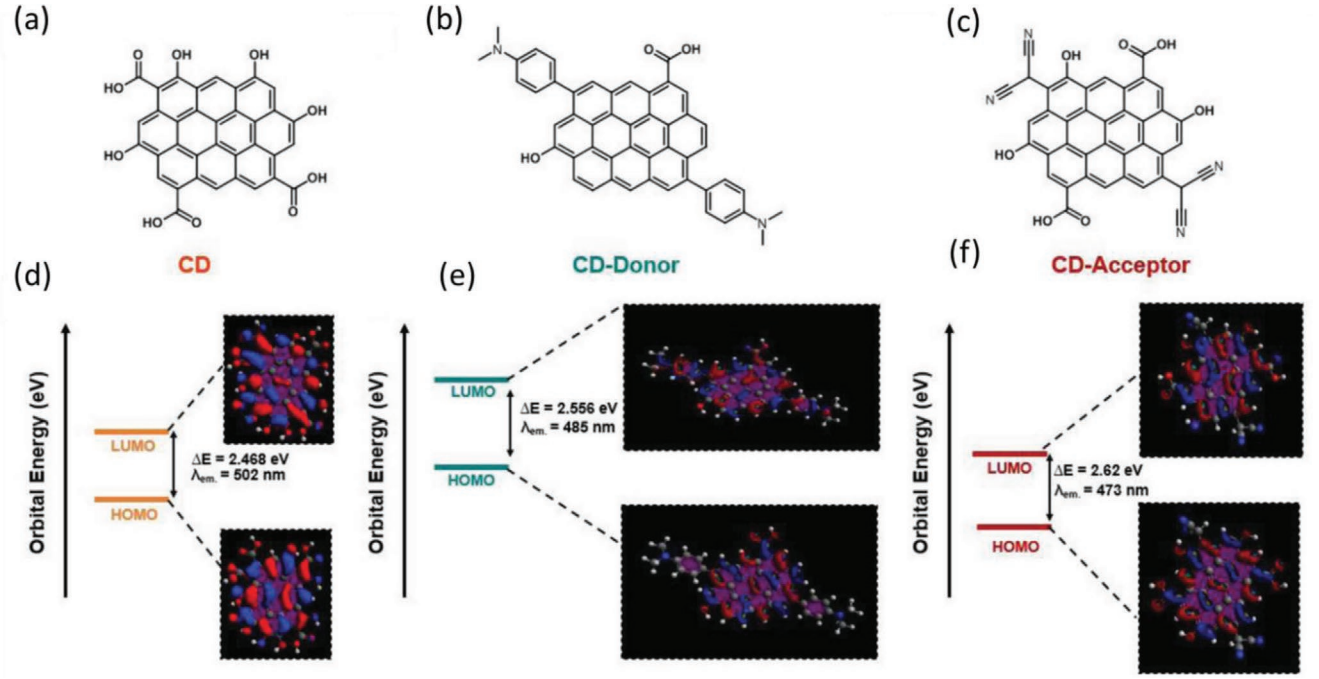

Figure 5. a) C-dots without any surface modification. b) C-dots modified with electron donor groups and c) C-dots modified with electron acceptors group. d–f) Density functional theory calculations performed on (a–c), respectively, to calculate the energy levels as well as HOMO and LUMO of the molecules. Reproduced with permission.[59] Copyright 2019, Wiley-VCH.

structural modification can force C-dots to either act as electron-acceptors or electron donor entities. As shown in Figure 5d, the addition of these donor and acceptor groups to C-dots leads to changes in HOMO and LUMO energy levels. CD-donor HOMO and LUMO were determined at higher energy levels compared to both CD and CD-acceptor. It means that CD-donor can easily donate its photogenerated electrons to CD (thus making CD an electron acceptor) and CD-acceptor in their hybrid/mixture (CD-donor/CD, CD-donor-CD-acceptor). However, in a mixture of CD-acceptor and CD, CD acts as electron donor because its HOMO and LUMO are placed at a higher energy position compared to CD-acceptor. The conclusion is that CD possesses a bivalent redox character and can both act as electron acceptors or donors. In a mixture of CD-donor/CD-acceptor, the overall photophysical properties are governed by CD-acceptors. The authors suggested that this is due to potential energy/electron transfer between the two classes of CDs.

3.4. Upconversion Photoluminescence

Several studies indicate that C-dots exhibit upconversion photoluminescence properties. Upconversion is a multiple low-energy photon absorption process that ends up with the emission of a single high-energy photon thanks to the favorable electronic band structure of the absorber. This property is particularly useful during photocatalysis for many hybrid systems composed of C-dots attached to the surface of wide bandgap semiconductors such as TiO_2. C-dots can absorb long-wavelength visible or NIR light and then remit short-wavelength UV photons. These UV photons then induce photoexcitation in wide bandgap semiconductors (which are unable to absorb low energy radiation), thus enabling them indirectly to perform under visible light irradiation. Significant advancement in this field now allows upconversion of Vis/NIR radiation for C-dots. It is of particular importance as it allows harnessing ambient NIR radiations. However, efficiencies of the upconversion processes are still low and it is very hard to distinguish whether enhanced photodegradation efficiencies are originating from the upconversion phenomenon or from some of the other features of C-dots. Further, the mechanism of upconversion in C-dots is still not clear and several potential models are likely candidates such as two-photon absorption, antistokes PL, and auger process/thermal effect. On top of that, equipment artifacts can lead to deceitful results in upconversion PL measurements as well. Interference between second and first-order diffracted light originating from the Xe lamp excitation source can be misinterpreted as an upconversion effect within fluorescence spectrophotometer. High power coherent laser may avoid this artifact during PL measurements and is thus highly recommended for measurement related to C-dots, but care has to be put to avoid heat-induced modification of the C-dots.[60]

4. Photodegradation of Dyes

Photodegradation of dyes was first tested with hybrid composites of C-dots and wide bandgap semiconductors. The first study was reported by Li et al. in 2010.[61] The authors tested bare CQDs and CQDs/TiO_2 composite for methylene blue (MB) dye degradation under visible light irradiation. Bare CQDs showed no photodegradation of dye, while bare TiO_2 exhibited merely <5%. TiO_2 being an intrinsic wide bandgap

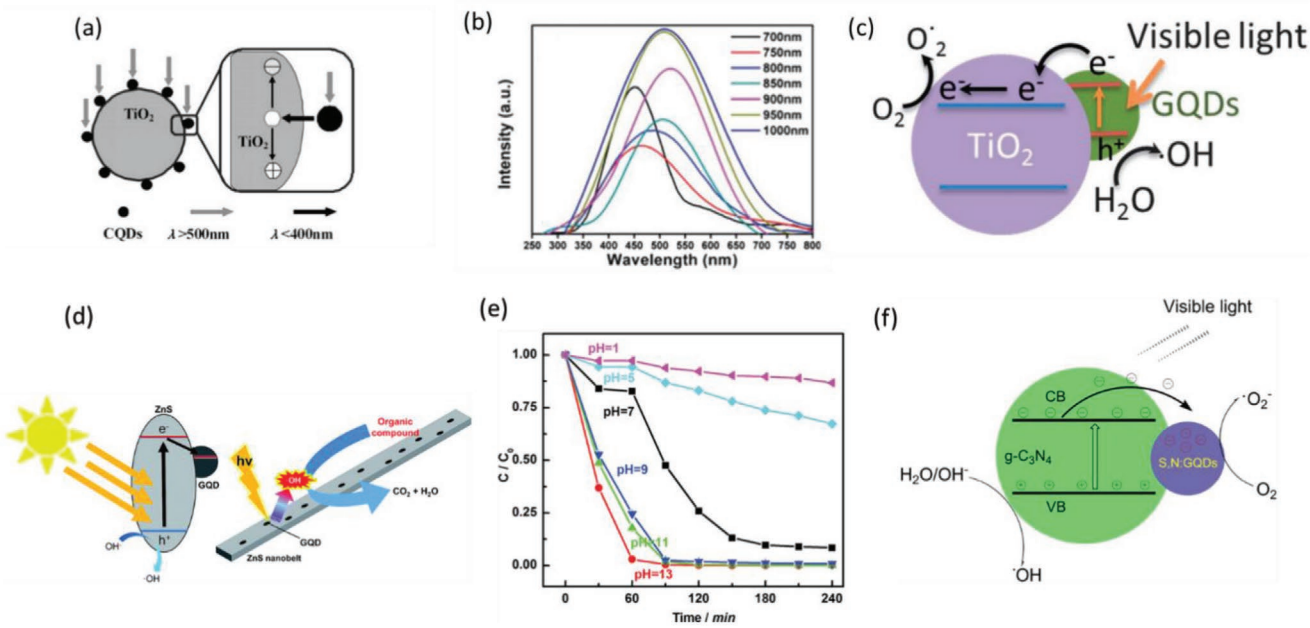

Figure 6. a) Possible catalytic mechanism for TiO_2/CQDs under visible light. Reproduced with permission.[69] Copyright 2010, Wiley-VCH. b) Upconverted PL spectra of CQDs. Reproduced with permission.[62] Copyright 2012, Royal Society of Chemistry. c) Possible photocatalyst mechanism of GQD/TiO_2 under visible light. Reproduced with permission.[63] Copyright 2013, Royal Society of Chemistry. d) Schematic for a plausible decomposition mechanism of an organic dye over a G/ZnS nanocomposite under light irradiation. Reproduced with permission.[66] Copyright 2016, Royal Society of Chemistry. e) Effect of pH on the adsorption and degradation rate of MB by xenon lamp irradiation. Reproduced with permission.[70] Copyright 2015, Royal Society of Chemistry. f) Proposed mechanism of the photocatalytic degradation of RhB for the g-C_3N_4/S,N:GQD composites. Reproduced with permission.[71] Copyright 2017, Elsevier.

semiconductor is only capable of absorbing a slight portion of visible light (<5%). Interestingly, CQDs/TiO_2 composite was able to photo reduce ≈100% MB after 25 min of irradiation. The enhanced photocatalytic activity is the result of upconversion of visible light assisted by CQDs. CQDs absorb visible light and then emit shorter-wavelength light, which is absorbed by TiO_2, where electron–hole pairs are generated (**Figure 6**a). Similarly, the up-conversion effect was observed in CQDs/Ag/Ag_3PO_4 by Zang et al.[62] CQDs, when excited by long-wavelength light in the range 700–1000 nm, emit shorter-wavelength light of 300–650 nm (Figure 6b). This high-energy light is then harvested by Ag_3PO_4 (2.4 eV bandgap) and resulted in 100% photodegradation of methyl orange (MO) dye. Similarly, Qu et al. prepared sulfur and nitrogen-doped graphene quantum dots and titanium dioxide composites (S,N-GQD/TiO_2) via physical mixing of S,N:GQDs and P25 TiO_2 with subsequent centrifugation and drying.[63] The composite was later tested for Rhodamine B photodegradation under visible light from a 300 W Xenon lamp with a UV cutoff filter ($\lambda > 400$ nm). Overall, S,N-GQD/TiO_2 composite outperformed commercial P25 TiO_2 ten times in terms of photodegradation of dye. Contrary to previous reports, the authors suggested that GQDs absorb the radiation in the visible region, resulting in the generation of photogenerated electrons and holes. TiO_2 then accepted the photogenerated electrons from GQDs, thus facilitating the charge carrier separation process as depicted in Figure 6c. The separated charge carriers then generated reactive radical species, which were responsible for the photodegradation of dye. A similar mechanism was reported for ZnO/S,N-GQD[64] and TiO2/S,N-GQDs.[65]

For other wide bandgap semiconductor hybrids of C-dots, when tested under UV–Vis light irradiation (where cutoff UV filter is not applied) for photodegradation, the charge dynamics regulating the electronic transfer is rather different, compared to what was depicted above, highlighting the dependence of the charge injection processes to the wavelength of the excitation radiation. In fact, under UV irradiation, the wide bandgap semiconductor can absorb radiation in the UV range, and here C-dots act as acceptors of photogenerated electrons, thus reducing the charge carrier recombination rates. C-dots then transfer these electrons to dissolved oxygen present in solution, which in turn results in the production of reactive oxygen radicals. The holes on the other side can be transferred to OH^- ions present in water, resulting in the production of hydroxyl radicals. These radicals are then responsible for the degradation of dyes as depicted in Figure 6d. This mechanism was demonstrated for many hybrids of C-dots with wide bandgap semiconductors such as ZnS/GQDs,[66] TiO_2/N-GQDs,[67] and SnO_2/GQDs.[68]

Photodegradation capabilities were also enhanced for relatively narrow bandgap semiconductors as well when integrated with C-dots. These semiconductors are capable of absorbing visible light, consequently generating electron-hole p airs. In such systems, C-dots act as electron scavengers and improve carrier separation. These electrons were then transferred to adsorbed ions to generate reactive radical species, which are responsible for degradation as shown in Figure 6f. Earlier work was inspired by metal porphyrins, which have unique photophysical properties that can be exploited for photodegradation.[70] GQDs can bind with these metals porphyrins via π–π

interaction. Zinc porphyrin GQDs hybrid (ZnPor/GQDs) is one example that has been successfully utilized to photodegrade MB under visible light (150W Xe lamp) for 1 h. The degradation efficiencies were 4%, 25%, and 95%, for GQDs, zinc porphyrin, and ZnPor/GQDs photocatalysts, respectively. The authors also tested commercial P25 TiO_2 under similar conditions, which achieved 95% degradation efficiency in 5 h, compared to 1 h for the ZnPor/GQDs system. Photodegradation efficiencies were also depending on the pH conditions as depicted in Figure 6e. Similarly, graphitic carbon nitride (g-C_3N_4)/S,N-GQDs composite was able to photodegrade 96% RhB within 90 min compared to 76% with bare g-C_3N_4 (Figure 6f).[71] Recent advancements in harvesting NIR radiation via C-dots encouraged their utilization in hybrid photodegradation catalysts. Hou et al. synthesized CQDs/H-γTaON hybrids that can enhance the UV–Vis–NIR broad-spectrum active photodegradation of RhB and acid orange 7 compared to bare H-γTaON.[61] CQDs can significantly enhance absorption in the NIR region in CQDs/H-γTaON hybrids. Moreover, upconversion PL properties of CQDs allow for the generation of even more electron-hole pairs, which can induce the formation of reactive radical species.

Even with the immense progress in the synthesis of C-dots, there are still few reports where bare C-dots were directly used as active photocatalytic material. The first effort regarding exclusive utilization of C-dots as photocatalyst was reported by Umrao et al.[72] Multilayered graphene quantum dots (MLGQDs) were used for photodegradation of MB under green and blue light. The enhanced degradation efficiency of 93.3% was observed in green light versus 89.4% under blue light for a total duration of 60 min. Ab initio theoretical calculations reveal the formation of intermediate products via the transfer of a proton from the hydroxyl group of MLGQDs to MB monomers. These intermediate products then degrade into benign products via reaction with highly reactive OH radicals. Sabet et al. produced N-doped CQDs from the grass with a bandgap of 2.5 eV, which were capable of absorbing light in both visible and UV regions. These dots were then utilized for the photodegradation of five dyes namely acid blue, acid red, eosin Y, eriochrome black T, methyl orange, and MB. N-doped CQDs generated electron–hole pairs upon irradiation, which in turn created reactive oxide species within aqueous media containing dye molecules. The authors concluded that reactive oxide species were the main responsible for the degradation of dyes.[73] Likewise, Aghamali et al. reported the excitation independent 95% quantum yield of N-doped CQDs. Produced quantum dots exhibit good photodegradation of MB under natural sunlight conditions via in situ generations of H_2O_2 in the reaction media.[9] Mg-N-embedded carbon dots (Mg-N/C-dots) synthesized from bougainvillea plant leaves extract exhibited excitation-independent red emissions at ≈678 nm with a quantum yield of ≈40%.[74] The eventual utilization of Mg-N/C-dots for MB degradation proved to be six times superior under natural sunlight compared to the artificial visible light from a 100 W tungsten bulb as shown in **Figure 7**a. Figure 7b indicates that Mg-N/C-dots were able to successfully generate electron–hole pairs under sunlight irradiation, which were eventually utilized to photodegrade MB.

In a recent study, Ibarbia et al. compared the photocatalytic properties of three different types of GQDs for the degradation of RhB.[75] Evaluations were performed for GQDs with similar sizes but varying compositions and bandgaps (ranging from

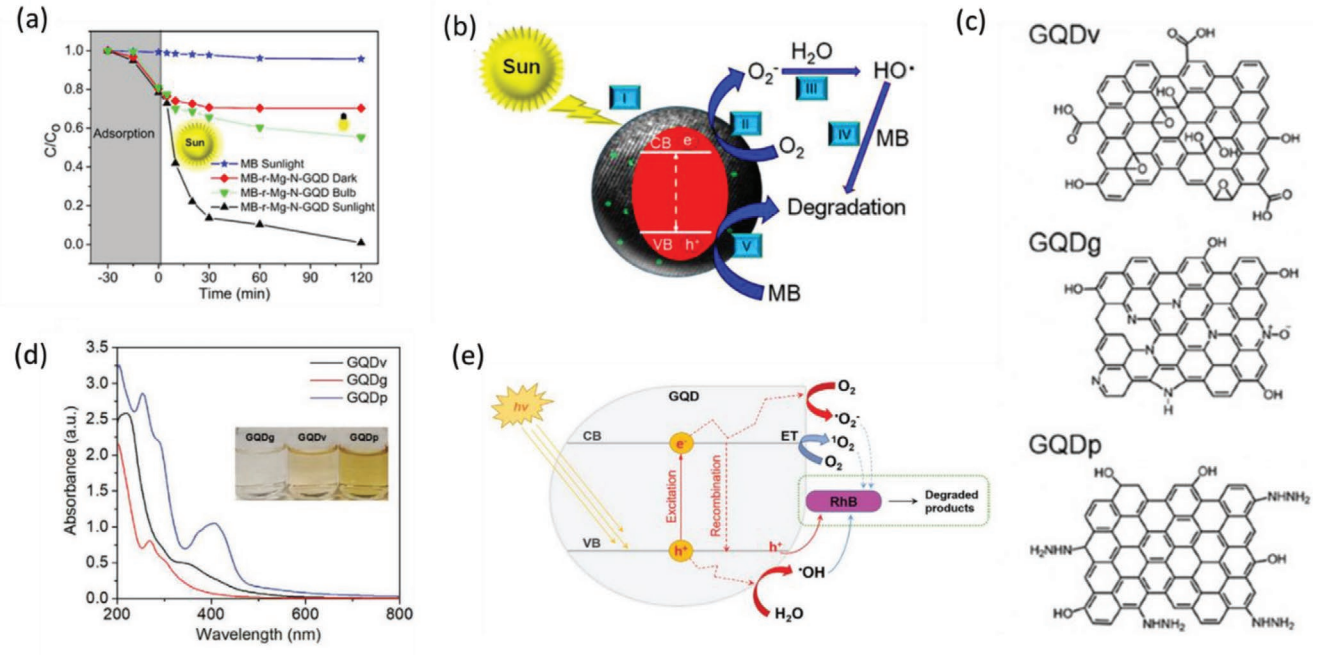

Figure 7. a) Plot of (C/C_0) versus time for MB photodegradation by r-Mg-N-CD under different conditions. b) Schematic representation of the mechanism of photodegradation of MB by r-Mg-N-CD showing several possible pathways (*I*–*V*) for dye degradation. a,b) Reproduced with permission.[74] Copyright 2018, American Chemical Society. c) Chemical structures of different GQDs prepared via different methods; GQDv via oxidative cutting of carbon black, QGDg via hydrothermal pyrolysis, and GQDp via hydrothermal condensation of pyrene. d) UV–Vis absorption spectra and photographs (inset) of GQD solutions at 50 mg L^{-1}. e) Proposed photocatalytic degradation mechanism of RhB with GQDs. c–e) Reproduced with permission.[75] Copyright 2020, Wiley-VCH.

2.63 to 3.63 eV), as shown in Figure 7c,d. Varying the composition affected the surface charge and bandgap of the GQDs, which were the dominant factors in determining the photocatalytic capabilities of GQDs. A lower bandgap (2.63 eV) and higher surface negative charge (−56.0 mV) resulted in higher degradations rates. Attractive electrostatic forces between the dye and GQDs resulted in enhanced adsorption rates, which then facilitate its degradation at a light-absorbing event. Mechanistic studies into degradation pathways painted a rather complex picture as elaborated in Figure 7e. There are three possible pathways, by which GQDs can degrade the dye upon light excitation. First, given the excellent electron donor and acceptor behavior of GQD, some of these charge carriers can be transferred directly to adsorbed dye molecules and initiate their degradation. Second, reactive oxygen species ($^{\bullet}OH$ and $^{\bullet}O_2^-$) can be generated via the interaction of carriers with H_2O and dissolved O_2. Last, energetically excited GQD can transfer its energy to dissolved O_2 and produce singlet oxygen ($^1O_2$) and thus act as a photosensitizer. Authors found out that in their case, $^{\bullet}OH$ and $^1O_2$ played a major role in photodegradation while the contributions from $^{\bullet}O_2^-$ were minimal. Details of other photocatalysts utilized for degradation of dyes with C-dots are summarized in **Table 1**.

5. Photodegradation of Antibiotics and Drugs

Antibiotics are ubiquitous in modern clinical treatments due to their efficacy in killing harmful bacteria.[88–90] However, most antibiotics end up in waterways and traditional wastewater treatments are incapable of decomposing these drugs. This gives harmful bacteria, already present in the environment, sufficient time to develop resistance against these antibiotics.[91] Consequently, these antibiotics become ineffective against these pathogens when humans are infected. Thus, there is an urgent need to degrade these antibiotics before they enter waterways. Photodegradation offers a unique solution, in this case, owing to the ubiquitous availability of sunlight.

To date, there is no report in literature where bare carbon dots were utilized for the photodegradation of antibiotics. Only C-dots hybrids thus far fit the purpose. However, there are few reports where C-dots were utilized as active light-harvesting material and generated electron–hole pairs transferred to other catalysts. For instance, Sharma et al. fabricated trimetallic La/Cu/Zr C-dots hybrids and tested them for photodegradation of malachite green dye and ampicillin antibiotic, under visible light irradiation.[92] Trimetallic nanoparticles hybrid fabrication resulted in bandgap reduction of bare C-dots from 2.55 to 1.56 eV, which lead to enhanced light absorption in the visible region, the key to increase the photocatalytic properties of the composite. 96% of ampicillin antibiotic and 75% of malachite green was removed by La/Cu/Zr C-dots hybrid after 4 h of photodegradation. It is however worth noting that adsorption alone (in dark for 1 h) was able to remove 88% of ampicillin and 48% of dye, before 4 h of photodegradation, suggesting the important role of these materials in lowering the antibiotic/dye concentration in the wastewater.

As mentioned earlier, C-dots can accept photogenerated electrons produced by a semiconductor during a light-absorbing event and thus can effectively help in charge separation. Enhanced charge separation directly translates into boosted photodegradation capability of the photocatalyst. This is true in many hybrid photocatalysts with C-dots, which have been utilized to degrade various antibiotics. The first report regarding photodegradation of antibiotics with the aid of C-dot hybrid came out in 2015.[93] Authors tested Bi_2WO_4 and its hybrid with C-dots for rhodamine photodegradation of ciprofloxacin (CIP), tetracycline hydrochloride, endocrine-disrupting chemical bisphenol A, and B under visible light (**Figure 8**a–c). Bare Bi_2WO_4 is a relatively narrow bandgap semiconductor capable of absorbing radiation in the 200 to 450 nm range. In addition, it suffers greatly from high charge recombination rates. C-dots come in aid to scavenge photogenerated electrons under visible excitation of Bi_2WO_4. Further, C-dots extended the range of visible light absorption in its hybrid with Bi_2WO_4. As a result, C-dot/Bi_2WO_4 hybrid outperforms pure Bi_2WO_4 in terms of photodegradation activity against these pollutants. Authors indicate that effective charge separation was the result of excellent electron-accepting capabilities of C-dots due to the presence of numerous conjugated π-bonds on their surface. Mechanistic studies show that photogenerated electrons were then transferred to dissolved oxygen and thus lead to the formation of $^{\bullet}O_2^-$, which acts as active species for photodegradation of organic pollutants in combination with h^+. Similar enhanced results were reported for ZnS/ C-dots hybrid (compared to bare ZnS) for photodegradation of MB, rhodamine B, and the antibiotic CIP hydrochloride.[94] Other studies that describe similar enhanced photodegradation due to effective charge separation mechanism and support of C-dots to absorb visible light include GQDs/mpg-C_3N_4 composites and TiO_2/carbon-dot nanocomposites.[95,96]

Effective charge separation can be estimated indirectly via observation of a relative reduction in PL intensities of hybrid photocatalysts. For instance, in Figure 8d, relatively reduced PL intensities were observed for CdSe/C-dots/r-GO and CdSe/C-dots compared to bare CdSe.[97] Consequently, CdSe/C-dots/r-GO and CdSe/C-dots showed enhanced tetracycline hydrochloride (TC·HCl) photodegradation compared to bare CdSe. Authors conclude that the addition of r-GO resulted in increased surface area, facilitating the adsorption of antibiotic, which was subsequently photodegraded.

Photodegradation of antibiotics conducted under just UV-light also shows enhanced efficiencies for C-dots hybrids, compared to bare semiconductors, a case consistent with dye photodegradation. C-dots strongly absorb in UV range, which results in the generation of even more electron–hole pairs, now contributing to photodegradation. Further, C-dots can accept photogenerated electron–hole pairs and enhance efficiencies. For instance, Di et al. tested (N-CQDs)/$BiPO_4$ hybrid and bare $BiPO_4$ for photodegradation of antibiotic CIP, enrofloxacin, tetracycline, and phenol 4-chlorophenol under UV irradiation.[98] 87.5% of CIP was photodegraded with (N-CQDs)/$BiPO_4$ compared to 64.4% with $BiPO_4$ under identical testing conditions. Electron spin resonance (ESR) signals of spin-trapped radicals analysis showed (Figure 8e) that photoexcited electrons were transferred to adsorbed oxygen transforming it into a reactive $^{\bullet}O_2^-$ radical. Further, electron paramagnetic resonance (EPR) data showed (Figure 8f) that molecular oxygen can better be

Table 1. C-dots based photocatalyst for dye photodegradation.

Catalysts	Pollutant	Light source	Role of C-dots	Degradation entities	Efficiency/time	Refs.
MLGQDs	MB	Green light	Photocatalyst	e^-, $^{\bullet}OH$	93.3%, 60 min	[72]
GQDs	New Fuchsin dye	Visible light	Photocatalyst	$^{\bullet}O_2^-$, $^{\bullet}OH$	95.0%, 110 min	[76]
Polymer-modified GQDs	MB	300 W Xe lamp	Photocatalyst	$^{\bullet}O_2^-$, $^{\bullet}OH$	45%, 100 min	[77]
GQDs	MB	Sunlight	Photocatalyst	$^{\bullet}O_2^-$, $^{\bullet}OH$	45%, 100 min	[78]
GQDs	RhG	Sunlight	Photocatalyst	$^{\bullet}O_2^-$, $^{\bullet}OH$	80%, 80 min	[79]
N-CQDs	MB	Sunlight	Photocatalyst	$^{\bullet}O_2^-$, $^{\bullet}OH$	~ 97%, 6 h	[9]
Mg-N-CQDs	MB	Sunlight	Photocatalyst	$^{\bullet}O_2^-$, $^{\bullet}OH$	99.1%/120 min	[74]
C-dots	MB	Sunlight	Photocatalyst	$^{\bullet}O_2^-$, $^{\bullet}OH$	43%/10 h	[80]
CQDs	MB	Vis	Photocatalyst	$^{\bullet}O_2^-$, $^{\bullet}OH$	≈99.5%/130 min	[81]
N-CQDs	Acid blue, acid red, eosin Y, eriochrome black T, MO, MB	UV irradiation	Photocatalyst	$^{\bullet}O_2^-$, $^{\bullet}OH$	100%/ 30 min for all dyes	[73]
GQDs	RhB	Vis	Photocatalyst	$^{\bullet}O_2^-$, $^{\bullet}OH$	55%/360 min	[75]
GQDs	MB, MO	Vis	Photocatalyst	$^{\bullet}O_2^-$, $^{\bullet}OH$	79.4%/120 min 52%/120 min	[82]
CQDs/Cu_2O	MB	NIR	Upconversion	$^{\bullet}O_2^-$, $^{\bullet}OH$	90%/240 min	[83]
CQDs/TiO_2	MB	Vis	Upconversion	$^{\bullet}O_2^-$, $^{\bullet}OH$	100%/25 min	[69]
CQDs/Ag/Ag_3PO_4	MO	Vis-NIR	Upconversion	$^{\bullet}O_2^-$, $^{\bullet}OH$	100%/10	[62]
N-GQDs/TiO_2	RhB	Vis	Light Absorption	$^{\bullet}O_2^-$, $^{\bullet}OH$	60%/100	[63]
CQDs/H-χ-TaON	RhB, acid orange	UV,Vis, NIR	Electron mediators, upconversion	$^{\bullet}O_2^-$, $^{\bullet}OH$	98%/140 min/UV 99%/100 min/UV 88%/140 min/Vis 90%/100 min/Vis 61%/140 min/NIR 66%/100 min/NIR	[61]
GQDs/ zinc porphyrin	MB	Vis	Electron mediators	$^{\bullet}O_2^-$, h^+	95%/60	[70]
GQDs/ZnS	RhB	UV-vis	Electron mediators	$^{\bullet}O_2^-$, $^{\bullet}OH$	≈82%/40	[66]
GQDs/SnO_2	MB	UV–vis	Electron mediators	$^{\bullet}O_2^-$, $^{\bullet}OH$	83.19%/150	[68]
S,N:GQD/ ZnO	RhB	Vis	Light absorber	$^{\bullet}O_2^-$, $^{\bullet}OH$	82.4%/250	[64]
N,S:GQD/TiO_2	MB	Vis	Light absorber, photosensitizer	$^{\bullet}O_2^-$, $^{\bullet}OH$	85.5%/240	[65]
N,GQDs/TiO_2	MB	UV	Electron mediators	$^{\bullet}O_2^-$, $^{\bullet}OH$	85%/70	[67]
N, S-GQDs/TiO_2 nanotubes	MO	Vis	Light absorber	$^{\bullet}O_2^-$, $^{\bullet}OH$	≈93%/240	[84]
S,N:GQD g-/C_3N_4	RhB	Vis	Electron mediators	$^{\bullet}O_2^-$, $^{\bullet}OH$	96%/90	[71]
PEDOT@ZnO@GQDs	MB, rhodamine 6G	UV, solar	Electron mediators, light absorption	$^{\bullet}O_2^-$, $^{\bullet}OH$	76.32%/400/UV 80.2%/400/VIS 69.3%/400/UV 85.2%/400/VIS	[85]
N-GQDs/TiO_2	MB	Sunlight	Light absorption	$^{\bullet}O_2^-$, $^{\bullet}OH$	100%/150 min	[86]
Fe_3O_4@N,S-GQDs	Victoria blue R dye	UV	Light absorption	$^{\bullet}O_2^-$, $^{\bullet}OH$	96.68%/120 min	[87]

active into its radical form over N-CQDs, which eventually lead to its higher concentrations. Similarly, Chen et al. showed enhanced photodegradation of RhB and cefradine under UV-light irradiation for TiO_2/C-dots hybrids compared to bare TiO_2.[57]

The incorporation of C-dots in heterojunctions of two distinct semiconductors further allows the manipulation of their properties, which results in enhanced photodegradation rates. Among three heterojunction schemes (type I, type II, and Z-scheme), Z-scheme promises maximum efficiency for the conversion of solar energy into useful chemical energy. Contrary to type II (**Figure 9**a), where electrons and hole movement from one semiconductor to another is restricted due to electrostatic repulsions, which ultimately results in overall lower redox potential, Z-scheme allows recombination of photogenerated electrons from one semiconductor to holes of the other

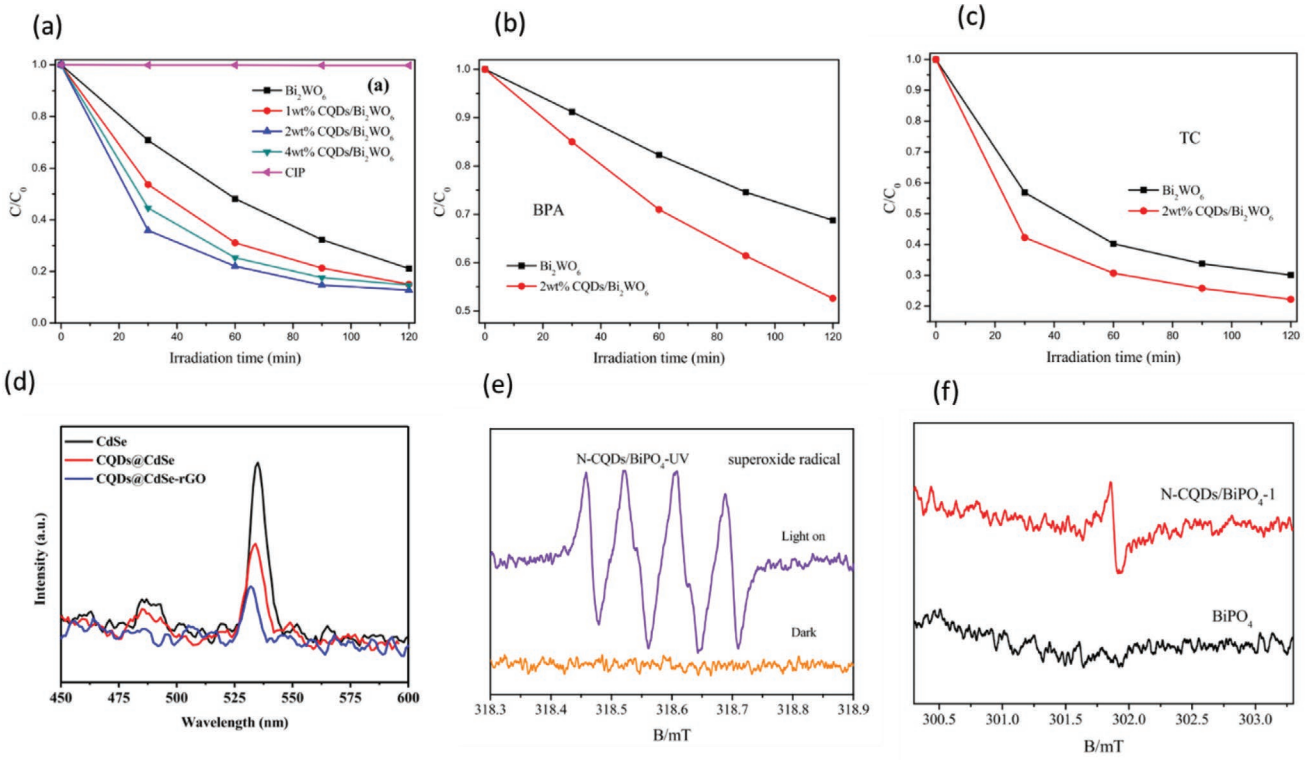

Figure 8. Photocatalytic degradation of a) CIP, b) BPA, and c) TC in the presence of pure Bi_2WO_6, CQDs/Bi_2WO_6 hybrid materials under visible light irradiation. a–c) Reproduced with permission.[93] Copyright 2015, Elsevier. d) Solid fluorescence spectra of CdSe, CQDs/CdSe, and CQDs/CdSe-rGO (5 wt% GO).[97] Reproduced with permission.[97] Copyright 2021, Elsevier. e) ESR spectra of the DMPO-$^{\bullet}O_2^-$ under UV light irradiation. f) Electron paramagnetic resonance (EPR) analysis of the pure $BiPO_4$ and N-CQDs/ $BiPO_4$ materials. e,f) Reproduced with permission.[98] Copyright 2017, Elsevier.

semiconductor(Figure 9b,c). This leads to lower recombination events within the individual semiconductor and directly translates into the accumulation of electrons and holes at opposite ends of valence and conduction bands of distinct semiconductors. These electrons and holes are now readily available for a redox reaction and hence the overall photodegradation efficiency is improved. To further enhance the efficiency of a Z-scheme heterojunction and to reduce the resistance between two semiconductors, conductive metals such as Pt and Ag are normally being utilized at the heterojunction interface. C-dots being excellent electronic conductors thus proved to be useful in this scenario. They offer advantages such as low cost and corrosion resistance compared to their metal counterparts. Jiang et al. tested photodegradation of benzocaine over CQD/$SnNb_2O_6$/BiOCl Z-scheme system compared to $SnNb_2O_6$ (SNO), BiOCl (BOC), and SNO/BOC Z-scheme system.[99] Z-scheme system with CQD (99.1% photodegradation efficiency) outperformed Z-scheme system without CQDs (80.8% photodegradation efficiency) within 90 min as shown in Figure 9d. Similarly, BiOCl/$BiVO_4$/N-GQDs followed Z-scheme charge transfer for photodegradation of Bisphenol A (BPA).[100] As shown in Figure 9e, after the formation of p–n heterojunction between p-type BiOCl and n-type $BiVO_4$, the build-up internal electric field can drive electrons from VB of BiOCl to VB of $BiVO_4$ resulting in accumulation of holes in VB of BiOCl. The VB (2.4 eV) of BiOCl is more positive than the redox potential of $^{\bullet}OH$ / OH^- (2.38 eV); hence, the holes can easily oxidize OH^- to $^{\bullet}OH$. Similarly, the CB of $BiVO_4$ (0.33 eV) is not negative enough to reduce oxygen to superoxide radical (–0.046 eV). Authors propose that under visible light, both N-GQDs and $BiVO_4$ were able to produce photogenerated electrons and holes; however, electrons from CB of $BiVO_4$ were transferred to VB of N-GQDs via Z-scheme. This resulted in the accumulation of more electrons in the CB of N-GQDs, which possess enough negative redox potential (–0.80 eV) to easily reduce oxygen into $^{\bullet}O_2^-$. The authors also suggested an internal Z-scheme within N-GQDs due to the presence of both p and n-type domains within their structure as shown in the inset of Figure 9e.

In a recent study, conducted by Hu et al., a Z-scheme charge transfer process was proposed between heterojunction of NCQDs and $Bi_2O_2CO_3$ while treating NCDs as a conventional semiconductor. Photodegradation of CIP was tested from UV to NIR region. Based on data obtained from band structure and reactive radical species, authors proposed that under UV-irradiation, hybrid catalyst followed a Z-scheme charge transfer mechanism, while under Vis/NIR irradiation, a normal type II charge transfer mechanism was adopted as shown in **Figure 10**. 5 wt% NCQDs/$Bi_2O_2CO_3$ showed 91.1% degradation efficiency of CIP under UV/Vis light irradiation, compared to 26.7% under visible and NIR light irradiation. In comparison, bare $Bi_2O_2CO_3$ (Bandgap 3.36 eV) showed 50.2% degradation under UV/Vis while merely 9% in VIS and no degradation under NIR light. Enhanced efficiency of NCQDs/$Bi_2O_2CO_3$ was attributed to upconversion and absorption of NIR/Vis by NCQDs. **Table 2** summarized the C-dots-based photocatalysts for photodegradation of antibiotics and other pollutants.

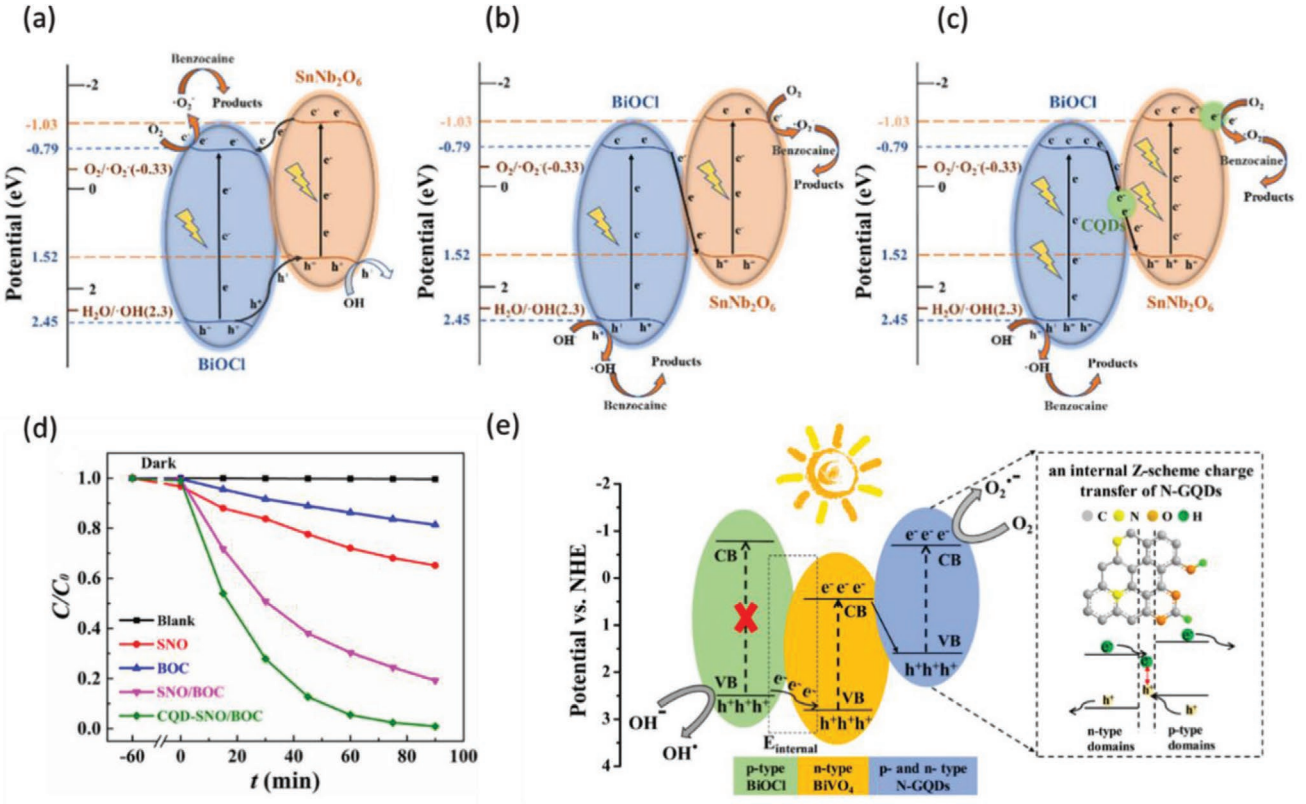

Figure 9. a) Possible photocatalytic mechanisms for a type II SNO/BOC heterojunction. b) Z-scheme of the SNO/BOC system. c) and the Z-scheme of the CQD-SNO/BOC system. d) Photocatalytic degradation of benzocaine under visible light irradiation. a–d) Reproduced with permission.[99] Copyright 2019, Elsevier. e) Z-scheme for electron transfer in BiOCl/$BiVO_4$/N-GQDs system. The inset shows the Z-scheme electron transfer within N-GQDs, due to its p- and n-type domains. Reproduced with permission.[100] Copyright 2017, American Chemical Society.

6. Other Aqueous Pollutants

Persistent organic pollutants are chemical compounds, which are resistant to environmental degradation through chemical, biological, and photolytic processes. Photodegradation of these environmentally persistent compounds is of utmost importance since they can continue to damage the environment for fairly long periods. C-dots and their hybrids have been tested for photodegradation of these compounds, but this field is still in its infancy and there are only a handful of reports available to date, which makes the development of the research in this direction urgent and timely. Hatefi et al. have tested the photodegradation of imipramine (a persistent organic pollutant) over bare GQDs under UV-irradiations.[126] Under optimized conditions, 80% of imipramine was photodegraded within a total duration of 80 min.

Haung et al. reported the photodegradation of perfluorooctane sulfonate ($C_8F_{17}SO_3H$, PFOS), another persistent and prevalent organic pollutant, under deep UV irradiation

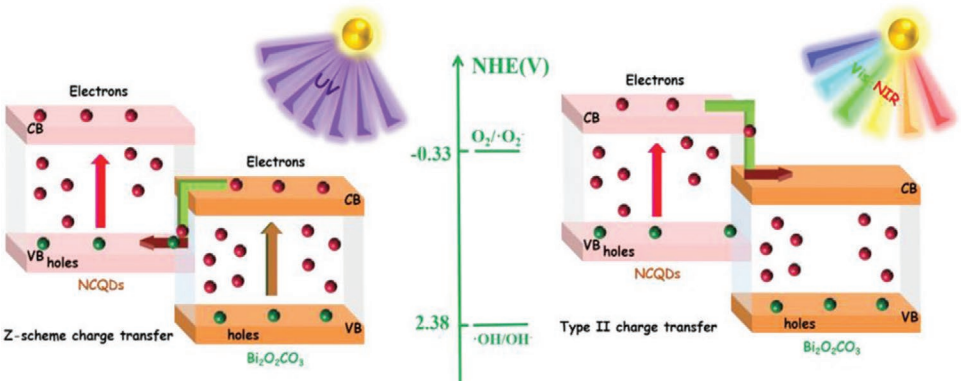

Figure 10. The schematic diagram of different NCQDs/BOC heterojunctions and two different roles of NCQDs under UV, visible, and NIR light irradiation. Reproduced with permission.[3] Copyright 2021, Elsevier.

Table 2. C-dots based photocatalysts for photodegradation of antibiotics and other pollutants.

Catalysts	Pollutant	Light source	Role of C-dots	Degradation radicals	Efficiency/time [min]	Refs.
CQDs/Bi_2O_6	CIP	Vis	Electron mediator	$^{\bullet}O_2^-$, h^+	87%/120	[72]
ZnS/CQD	CIP hydrochloride, RhB, MB	Vis	Electron mediator	$^{\bullet}O_2^-$, $^{\bullet}OH$	≈55%/, 120 ≈95%/ 120 ≈95%/60	[94]
CQDs/TiO_2	Cefradine, RhB	UV	Electron mediator	$^{\bullet}O_2^-$, $^{\bullet}OH$,	≈80%, 60 86.92%/120	[57]
La/Cu/Zr/CQDs TNCs	Ampicillin, malachite green	Vis	Photocatalyst	$^{\bullet}O_2^-$, $^{\bullet}OH$	96%/240 96%/240	[92]
CQDs)/CdSe/rGO	Tetracycline hydrochloride	Vis	Photocatalyst	$^{\bullet}O_2^-$, $^{\bullet}OH$, $^1O_2$	90%/60	[97]
N-CQDs/$BiPO_4$	CIP, enrofloxacin, tetracycline and phenol 4- chlorophenol	UV	Electron mediator	$^{\bullet}O_2^-$, $^{\bullet}OH$	87.5%/120 ≈60%/120 ≈70%,150 ≈82%/150	[98]
GQDs/$LaCoO_3$/ATP	Chlortetracycline, tetracycline hydrochloride, MB	Vis	Electron mediator	$^{\bullet}O_2^-$, h^+	≈47%/120 ≈78%/120 ≈94%/120	[101]
GQDs/mpg-C_3N_4	Tetracycline hydrochloride, RhB	Vis	Electron mediator	$^{\bullet}O_2^-$	67%/120 97%/120	[95]
CQDs/BiOBr	CIP, RhB	Vis	Electron mediator	$^{\bullet}O_2^-$, h^+	65.8%/180 94.3%/30	[102]
CQDs/BiOBr	Tetracycline hydrochloride, bisphenol A,RhB	Vis	Electron mediator	$^{\bullet}O_2^-$, $^{\bullet}OH$	60%/120 73%/150 91.8%/20	[103]
$BiVO_4$/N-CQDs/Ag_3PO_4	Tetracycline	Vis	Electron mediator	$^{\bullet}O_2^-$, $^{\bullet}OH$	59.8%/90	[104]
CD/$NiCo_2O_4$	Tetracycline	Vis	Electron mediator	$^{\bullet}O_2^-$, $^{\bullet}OH$	78%/60	[105]
α-Bi_2O_3/C-dots	Levofloxacin, indigo carmine dye	Vis	Electron mediator	$^{\bullet}O_2^-$, $^{\bullet}OH$	79%/120 86%/120	[106]
CQDs/ $PbBiO_2Cl$	CIP, tetracycline, bisphenol A	Vis	Electron mediator	$^{\bullet}O_2^-$, h^+	78.9%/75 74.3%/120 92%/360	[107]
CQDs/ $ZnIn_2S_4$/BiOC	Tetracycline	Vis/NIR	Electron mediator, upconversion	$^{\bullet}O_2^-$, $^{\bullet}OH$	82.3%/60 min under VIS 17.7%/180 min under IR	[108]
$BiVO_4$/Bi_3TaO_7/CDs	Tetracycline, amoxicillin and CIP	Vis	Electron mediator, upconversion	$^{\bullet}O_2^-$, $^{\bullet}OH$, h^+	91.7%/120 89.3%/120 87.1%/120	[109]
CQDs/$Bi_5Nb_3O_{15}$	Sarafloxacin	Vis	Electron mediator, Upconversion	$^{\bullet}OH$	86.8%/180	[110]
CQDs@Bi_2WO_6	Tetracycline, CIP, gatifloxacin	Vis	Upconversion, electron meditator	$^{\bullet}O_2^-$, $^{\bullet}OH$	≈90%/120 ≈90%/120 ≈90%/120	[111]
g-C_3N_4/CQDs	Diclofenac	Vis	Photosensitizer, electron mediator	$^{\bullet}O_2^-$, h^+	71.6%/60	[112]
$BiVO_4$/CNQDs/NCDs	Tetracycline, RhB	Vis	Upconversion, electron mediator	$^{\bullet}O_2^-$, $^{\bullet}OH$	≈75%/60 98%/100	[113]
CDs/$Bi_4O_5Br_2$	CIP	Vis	Broad absorption, electron mediator	$^{\bullet}O_2^-$, $^{\bullet}OH$	98%/100	[114]
CQDs/K_2Ti_6O13	Amoxicillin	UV, Vis	Broad absorption, electron meditator	h^+, $^{\bullet}OH$	100% in UV/ 90 73.6% in VIS/90	[115]
S-CQDs/hollow tubular g-C_3N_4 photocatalyst	Tetracycline	Vis	Electron meditator	$^{\bullet}O_2^-$, $^{\bullet}OH$, h^+	82.67%/60	[116]
CDs/$ZnSnO_3$	Tetracycline	Vis	Upconversion, electron mediator	$^{\bullet}O_2^-$, h^+	81.76%/60	[117]

Table 2. Continued.

Catalysts	Pollutant	Light source	Role of C-dots	Degradation radicals	Efficiency/time [min]	Refs.
CQDs/S@g-C_3N_4/B@g-C_3N_4	Chloramphenicol	Vis	Electron mediator	$^{\bullet}O_2^-$, $^{\bullet}OH$	92.4%/ 120	[118]
g- C_3N_4 /CQDs	Sulfachloropyridazine, RhB, MB, MO	UV/Vis	Broad absorption	$^{\bullet}O_2^-$, $^{\bullet}OH$	100%/90 80%/180 94%/180 95%/180	[119]
N-CQDs/BiOBr	CIP, RhB	Vis	Electron mediator	$^{\bullet}O_2^-$, $^{\bullet}OH$	65.8%/180 94.3%/30	[120]
ZnO/N,S-CQDs	CIP, cephalexin, malachite green	Simulated Solar,NIR	Upconversion, electron mediator	$^{\bullet}O_2^-$, $^{\bullet}OH$, h^+	92.9%/20/SS 92.9%/20/SS 72.8%/180/NIR	[121]
C-dots/$Sn_2Ta_2O_7$/SnO_2	Amoxicillin	Simulated solar	Upconversion, electron mediator	$^{\bullet}O_2^-$, $^{\bullet}OH$	88.3%/120	[122]
$Bi_2O_2CO_3$/ NCQDs	CIP	UV–Vis,Vis, NIR	Photosensitizer, upconversion, electron mediator	$^{\bullet}O_2^-$, $^{\bullet}OH$	91.1%/60/UV-VIS 92.8%/120/VIS 35.6%/360/NIR	[3]
GQD/$AgVO_3$	Ibuprofen	Vis ($\lambda > 420$ nm)	Electron mediator	$^{\bullet}O_2^-$, $^{\bullet}OH$	90%/120	[123]
SiC/GQDs	Perfluorooctane sulfonate	UV	Photocatalyst	$^{\bullet}O_2^-$, $^{\bullet}OH$	88.5%/20 h	[124]
Stainless-steel nanotubes/GQD	Phenanthrene	Vis	Photocatalyst	$^{\bullet}O_2^-$, $^{\bullet}OH$,	99.9%/240	[125]
GQDs	Imipramine	UV	Photocatalyst	$^{\bullet}O_2^-$, $^{\bullet}OH$	80%/80	[126]
NP-CD	Cr(VI) to Cr (III)	Sunlight	Photocatalyst	e^-	≈93%/10	[127]
CQD/CdS	Cr(VI) to Cr (III)	Vis	Photocatalyst	e^-	≈94%/10	[128]
3D CQDs/Graphene aerogel	Cr(VI) to Cr (III)	UV/Vis	Photocatalyst	e^-	91.3%/40	[12]

(5 W 254 nm UV lamp) conditions with SiC/GQDs and bare SiC.[124] The heterojunction allows the effective separation of generated electrons by GQDs under deep-UV conditions towards CB of SiC (**Figure 11**a). Long-chain PFOS was converted into shot chain perfluorocarboxylic acids on the surface of SiC surface by electronic transfer toward S—O group of PFOS. SiC showed minimal photodegradation compared to SiC/GQDs.

Photogenerated electrons over C-dots possess can also reduce toxic metallic ions. For instance, Bhati et al. reported photoreduction of Cr(VI) to Cr(III) in synthetic contaminated water by nitrogen-phosphorus-doped carbon dots.[127] Under natural sunlight conditions, orange-colored solution of highly toxic Cr(VI) turned into green-colored less toxic Cr(III), which can easily be removed via precipitation with the aid of NaOH (Figure 11b). Authors suggested that cumulative production of electrons and holes on nitrogen-phosphorus-doped carbon dots under irradiation resulted in the photoreduction of toxic Cr ions. Zhang et al. utilized CdS/CQDs for photoreduction of Cr(VI) to Cr(III) in saline waters with ≈94% removal efficiency within 10 min under visible light irradiation.[128]

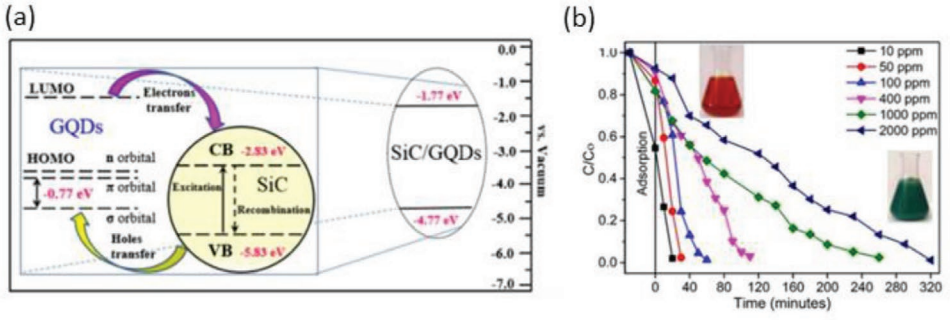

Figure 11. a) Schematics of electron and hole transfer in the SiC/GQDs heterojunction structure under UV light excitation. Reproduced with permission.[124] Copyright 2017, Elsevier. b) The plot of (C/C_0) versus time for Cr(VI) photoreduction by NP-CD under different concentrations of Cr(VI). Reproduced under the terms of a Creative Commons Attribution 4.0 International License.[127] Copyright 2019, The Auth.

7. Conclusions and Outlook

C-dots host unique photophysical and chemical properties in one package, which are hard to be rivaled by other nanomaterials at such a scale. C-dots possess upconversion properties and bivalent redox character can act as can as photocatalysts as well as photosensitizers and can harvest light ranging from UV, Vis, and NIR regions. Their nonmetallic and chemically inert nature along with their ease of synthesis from a variety of sources made them an ideal candidate for photodegradation of pollutants from aqueous environments. Bare C-dots are capable of removing organic dyes under different irradiation conditions. Photodegradation of drugs, antibiotics, and other long-chain organic pollutants can also be achieved with C-dots and their hybrids with semiconductors. This is one of the most promising directions for future research, which may provide useful strategies for water purification from drugs, antibiotics, and long-chain organics. C-dots offer a variety of features, when combined with semiconductors in their hybrids, such as light absorption in the region where the semiconductor is unable to harvest the light, upconversion photoluminescence, effective charge carrier separation, and sometimes photosensitization properties. Despite tremendous progress in the utilization of C-dots and their hybrids towards removal/photodegradation of environmental pollutants, there remain several challenges, which are curial for further advancement of the field, which is relatively new and has strong potential for fast development.

1. Standardization in C-dots purification methods is needed at this point, since diverse synthetic approaches can produce a host of molecular entities that can mimic like C-dots and interfere with photophysical observations.
2. Solid experimental confirmations are yet required regarding absorption-emission properties of C-dots under UV, Vis, and IR excitation, since their optoelectronic properties are not yet univocally understood. Controversies surrounding quantum confinement in C-dots are also needed to be cleared out.
3. Precise control over structural aspects of C-dots is needed since a variety of functional groups can influence heavily their chemical and photophysical properties. This precise control will allow to specifically target the photodegradation of certain pollutants entities in complex aqueous environments.
4. More recently, the work on single-atom catalysis has received huge attention from the research community, owing to its exceptional performance in diverse areas. A variety of 2D materials has been explored as potential support materials for anchoring single metal atoms. C-dots can potentially host a series of elements as single atoms, owing to the availability of diverse surface functionalities. Research in this area would not only benefit for the photodegradation of environmental pollutants, but also presents exciting opportunities in other areas of science.
5. Since C-dots are 2D in nature, fabrication of superlattices of C-dots with other 2D material quantum dots would be a viable strategy to further enhance their photodegradation capabilities.
6. Regardless of significant advances made in the field of hybrids of C-dots and their applications in photodegradation, sole C-dots still did not get much attention from the research community. Recent studies have shown that bare C-dots can also be viable candidates for photodegradation purposes. However, more fundamental studies and in-depth analysis are needed on this subject before realizing the full potential of bare C-dots in the photodegradation of aqueous pollutants.

Although C-dots hybrids proved to be useful thus far for photodegradation of aqueous pollutants, the inorganic and potentially toxic nature of some of the utilized semiconductors can potentially be harmful rather than beneficial to the environment. Thus, further investigations are needed to utilize solely C-dots for the photodegradation of these pollutants. In addition, to further progress the field towards more practical applications and lab-to-fab transition, scalable and cost-effective methods are need for the production of C-dots and their hybrids.

Finally, a critical point is the assessment of the environmental impact of C-dots, which is still to be achieved over larger scales. This is a very important point since these materials are sub-nanometer in dimensions and can disseminate rather quickly once released into the environment. A recent study suggests that C-dots, when irradiated with light for eight days, can degrade into molecules that are toxic to both normal (HEK-293) and cancerous (HeLa and HepG2) human cells and thus can pose serious challenges to the environment.[129]

For this reason, while intense research has been carried out on the use of C-dots in a series of applications in photocatalysis, environmental remediation, and energy conversion, with outstanding results, a systematic investigation is needed on their safe management to offer a solid ground for a lab-to-fab transition of this highly innovative class of materials.

Conflict of Interest

The authors declare no conflict of interest.

Keywords

antibiotics photodegradation, carbon dots, photocatalysis, photodegradation

Received: March 15, 2021
Revised: May 1, 2021
Published online:

[1] X. Zhang, M. Jiang, N. Niu, Z. Chen, S. Li, S. Liu, J. Li, *ChemSusChem* **2018**, *11*, 11.
[2] N. V. Tepliakov, E. V. Kundelev, P. D. Khavlyuk, Y. Xiong, M. Y. Leonov, W. Zhu, A. V. Baranov, A. V. Fedorov, A. L. Rogach, I. D. Rukhlenko, *ACS Nano* **2019**, *13*, 10737.
[3] X. Hu, H. Zhao, Y. Liang, F. Chen, J. Li, R. Chen, *Chemosphere* **2021**, *264*, 128434.
[4] S. Asadzadeh-Khaneghah, A. Habibi-Yangjeh, M. Shahedi Asl, Z. Ahmadi, S. Ghosh, *J. Photochem. Photobiol., A* **2020**, *392*, 112431.
[5] S. Tao, S. Zhu, T. Feng, C. Xia, Y. Song, B. Yang, *Mater. Today Chem.* **2017**, *6*, 13.
[6] S. Asadzadeh-Khaneghah, A. Habibi-Yangjeh, K. Nakata, *J. Photochem. Photobiol., A* **2019**, *374*, 161.

[7] A. Habibi-Yangjeh, S. Feizpoor, D. Seifzadeh, S. Ghosh, *Sep. Purif. Technol.* **2020**, *238*, 116404.
[8] S. Mondal, A. Yucknovsky, K. Akulov, N. Ghorai, T. Schwartz, H. N. Ghosh, N. Amdursky, *J. Am. Chem. Soc.* **2019**, *141*, 15413.
[9] A. Aghamali, M. Khosravi, H. Hamishehkar, N. Modirshahla, M. A. Behnajady, *J. Lumin.* **2018**, *201*, 265.
[10] A. Yadegari, J. Khezri, S. Esfandiari, H. Mahdavi, A. A. Karkhane, R. Rahighi, R. Heidarimoghadam, L. Tayebi, E. Hashemi, A. Farmany, *Colloids Surf., B* **2019**, *184*, 110543.
[11] S. Feizpoor, A. Habibi-Yangjeh, D. Seifzadeh, S. Ghosh, *Sep. Purif. Technol.* **2020**, *248*, 116928.
[12] R. Wang, K. Q. Lu, F. Zhang, Z. R. Tang, Y. J. Xu, *Appl. Catal., B* **2018**, *233*, 11.
[13] M. S. Swapna, S. Sankararaman, *Int. J. Mater. Sci.* **2017**, *12*, 541.
[14] X. Hou, Y. Hu, P. Wang, L. Yang, M. M. Al Awak, Y. Tang, F. K. Twara, H. Qian, Y. P. Sun, *Carbon* **2017**, *122*, 389.
[15] S. Cailotto, R. Mazzaro, F. Enrichi, A. Vomiero, M. Selva, E. Cattaruzza, D. Cristofori, E. Amadio, A. Perosa, *ACS Appl. Mater. Interfaces* **2018**, *10*, 40560.
[16] H. Yu, R. Shi, Y. Zhao, G. I. N. Waterhouse, L. Z. Wu, C. H. Tung, T. Zhang, *Adv. Mater.* **2016**, *28*, 9454.
[17] H. Ding, X. X. Zhou, J. S. Wei, X. B. Li, B. T. Qin, X. B. Chen, H. M. Xiong, *Carbon* **2020**, *167*, 322.
[18] C. Long, Z. Jiang, J. Shangguan, T. Qing, P. Zhang, B. Feng, *Chem. Eng. J.* **2021**, *406*, 126848.
[19] H. Zhao, G. Liu, S. You, F. V. A. Camargo, M. Zavelani-Rossi, X. Wang, C. Sun, B. Liu, Y. Zhang, G. Han, A. Vomiero, X. Gong, *Energy Environ. Sci.* **2021**, *14*, 396.
[20] D. Benetti, E. Jokar, C. H. Yu, A. Fathi, H. Zhao, A. Vomiero, E. Wei-Guang Diau, F. Rosei, *Nano Energy* **2019**, *62*, 781.
[21] A. Nair, J. T. Haponiuk, S. Thomas, S. Gopi, *Biomed. Pharmacother.* **2020**, *132*, 110834.
[22] Y. Zhou, L. Liu, Y. Shen, L. Wu, L. Yu, F. Liang, J. Xi, *Chem. Commun.* **2017**, *53*, 7565.
[23] P. Zhang, D. Bin, J. S. Wei, X. Q. Niu, X. B. Chen, Y. Y. Xia, H. M. Xiong, *ACS Appl. Mater. Interfaces* **2019**, *11*, 14085.
[24] K. O. Boakye-Yiadom, S. Kesse, Y. Opoku-Damoah, M. S. Filli, M. Aquib, M. M. B. Joelle, M. A. Farooq, R. Mavlyanova, F. Raza, R. Bavi, B. Wang, *Int. J. Pharm.* **2019**, *564*, 308.
[25] S. Zhu, Y. Song, J. Wang, H. Wan, Y. Zhang, Y. Ning, B. Yang, *Nano Today* **2017**, *13*, 10.
[26] E. Dervishi, Z. Ji, H. Htoon, M. Sykora, S. K. Doorn, *Nanoscale* **2019**, *11*, 16571.
[27] D. Huang, H. Zhou, Y. Wu, T. Wang, L. Sun, P. Gao, Y. Sun, H. Huang, G. Zhou, J. Hu, *Carbon* **2019**, *142*, 673.
[28] Y. Yan, D. Zhai, Y. Liu, J. Gong, J. Chen, P. Zan, Z. Zeng, S. Li, W. Huang, P. Chen, *ACS Nano* **2020**, *14*, 1185.
[29] H. H. Kim, Y. J. Lee, C. Park, S. Yu, S. O. Won, W. S. Seo, C. Park, W. K. Choi, *Part. Part. Syst. Charact.* **2018**, *35*, 1800080.
[30] T. J. Pillar-Little, N. Wanninayake, L. Nease, D. K. Heidary, E. C. Glazer, D. Y. Kim, *Carbon* **2018**, *140*, 616.
[31] K. Dimos, F. Arcudi, A. Kouloumpis, I. B. Koutselas, P. Rudolf, D. Gournis, M. Prato, *Nanoscale* **2017**, *9*, 10256.
[32] F. Rigodanza, L. Đorđević, F. Arcudi, M. Prato, *Angew. Chem.* **2018**, *130*, 5156.
[33] Q. Liu, Y. Zhou, J. Lu, Y. Zhou, *Chemosphere* **2020**, *241*, 125043.
[34] K. P. Gopinath, N. V. Madhav, A. Krishnan, R. Malolan, G. Rangarajan, *J. Environ. Manage.* **2020**, *270*, 110906.
[35] U. A. Rani, L. Y. Ng, C. Y. Ng, E. Mahmoudi, *Adv. Colloid Interface Sci.* **2020**, *278*, 102124.
[36] N. Dhenadhayalan, K. C. Lin, T. A. Saleh, *Small* **2020**, *16*, 1905767.
[37] R. Wang, K. Q. Lu, Z. R. Tang, Y. J. Xu, *J. Mater. Chem. A* **2017**, *5*, 3717.
[38] S. Sharma, V. Dutta, P. Singh, P. Raizada, A. Rahmani-Sani, A. Hosseini-Bandegharaei, V. K. Thakur, *J. Cleaner Prod.* **2019**, *228*, 755.
[39] C. Michelin, N. Hoffmann, *ACS Catal.* **2018**, *8*, 12046.
[40] F. Ehrat, S. Bhattacharyya, J. Schneider, A. Löf, R. Wyrwich, A. L. Rogach, J. K. Stolarczyk, A. S. Urban, J. Feldmann, *Nano Lett.* **2017**, *17*, 7710.
[41] C. J. Reckmeier, J. Schneider, Y. Xiong, J. Häusler, P. Kasák, W. Schnick, A. L. Rogach, *Chem. Mater.* **2017**, *29*, 10352.
[42] L. Shahriary, A. A. Athawale, *Int. J. Renewable Energy Environ. Eng.* **2014**, *2*, 58.
[43] F. Yuan, Z. Wang, X. Li, Y. Li, Z. Tan, L. Fan, S. Yang, *Adv. Mater.* **2017**, *29*, 1604436.
[44] Z. Tian, X. Zhang, D. Li, D. Zhou, P. Jing, D. Shen, S. Qu, R. Zboril, A. L. Rogach, *Adv. Opt. Mater.* **2017**, *5*, 1700416.
[45] F. A. Permatasari, H. Fukazawa, T. Ogi, F. Iskandar, K. Okuyama, *ACS Appl. Nano Mater.* **2018**, *1*, 2368.
[46] B. Geng, W. Shen, F. Fang, H. Qin, P. Li, X. Wang, X. Li, D. Pan, L. Shen, *Carbon* **2020**, *162*, 220.
[47] Y. Song, S. Zhu, S. Zhang, Y. Fu, L. Wang, X. Zhao, B. Yang, *J. Mater. Chem. C* **2015**, *3*, 5976.
[48] S. Khan, A. Sharma, S. Ghoshal, S. Jain, M. K. Hazra, C. K. Nandi, *Chem. Sci.* **2017**, *9*, 175.
[49] J. B. Essner, J. A. Kist, L. Polo-Parada, G. A. Baker, *Chem. Mater.* **2018**, *30*, 1878.
[50] N. A. Romero, D. A. Nicewicz, *Chem. Rev.* **2016**, *116*, 10075.
[51] Y. Zhang, T. S. Lee, J. L. Petersen, C. Milsmann, *J. Am. Chem. Soc.* **2018**, *140*, 5934.
[52] S. Wu, R. Zhou, H. Chen, J. Zhang, P. Wu, *Nanoscale* **2020**, *12*, 5543.
[53] V. Strauss, J. T. Margraf, K. Dirian, Z. Syrgiannis, M. Prato, C. Wessendorf, A. Hirsch, T. Clark, D. M. Guldi, *Angew. Chem., Int. Ed.* **2015**, *54*, 8292.
[54] F. Arcudi, V. Strauss, L. Đorđević, A. Cadranel, D. M. Guldi, M. Prato, *Angew. Chem., Int. Ed.* **2017**, *56*, 12097.
[55] Z. Zhang, G. Yi, P. Li, X. Zhang, H. Fan, Y. Zhang, X. Wang, C. Zhang, *Nanoscale* **2020**, *12*, 13899.
[56] K. W. Chu, S. L. Lee, C. J. Chang, L. Liu, *Polymers* **2019**, *11*, 689.
[57] J. Chen, J. Shu, Z. Anqi, H. Juyuan, Z. Yan, J. Chen, *Diamond Relat. Mater.* **2016**, *70*, 137.
[58] G. Sodeifian, R. Behnood, *J. Inorg. Organomet. Polym. Mater.* **2020**, *30*, 1266.
[59] I. Srivastava, J. S. Khamo, S. Pandit, P. Fathi, X. Huang, A. Cao, R. T. Haasch, S. Nie, K. Zhang, D. Pan, *Adv. Funct. Mater.* **2019**, *29*, 1902466.
[60] M. Han, S. Zhu, S. Lu, Y. Song, T. Feng, S. Tao, J. Liu, B. Yang, *Nano Today* **2018**, *19*, 201.
[61] J. Hou, H. Cheng, C. Yang, O. Takeda, H. Zhu, *Nano Energy* **2015**, *18*, 143.
[62] H. Zhang, H. Huang, H. Ming, H. Li, L. Zhang, Y. Liu, Z. Kang, *J. Mater. Chem.* **2012**, *22*, 10501.
[63] D. Qu, M. Zheng, P. Du, Y. Zhou, L. Zhang, D. Li, H. Tan, Z. Zhao, Z. Xie, Z. Sun, *Nanoscale* **2013**, *5*, 12272.
[64] A. Cai, X. Wang, Y. Qi, Z. Ma, *Appl. Surf. Sci.* **2017**, *391*, 484.
[65] K. Shen, X. Xue, X. Wang, X. Hu, H. Tian, W. Zheng, *RSC Adv.* **2017**, *7*, 23319.
[66] S. Ham, Y. Kim, M. J. Park, B. H. Hong, D. J. Jang, *RSC Adv.* **2016**, *6*, 24115.
[67] H. Safardoust-Hojaghan, M. Salavati-Niasari, *J. Cleaner Prod.* **2017**, *148*, 31.
[68] B. Quan, W. Liu, Y. Liu, Y. Zheng, G. Yang, G. Ji, *J. Colloid Interface Sci.* **2016**, *481*, 13.
[69] H. Li, X. He, Z. Kang, H. Huang, Y. Liu, J. Liu, S. Lian, C. H. A. Tsang, X. Yang, S. T. Lee, *Angew. Chem., Int. Ed.* **2010**, *49*, 4430.
[70] Q. Lu, Y. Zhang, S. Liu, *J. Mater. Chem. A* **2015**, *3*, 8552.
[71] A. Cai, Q. Wang, Y. Chang, X. Wang, *J. Alloys Compd.* **2017**, *692*, 183.

[72] S. Umrao, P. Sharma, A. Bansal, R. Sinha, R. K. Singh, A. Srivastava, *RSC Adv.* **2015**, *5*, 51790.
[73] M. Sabet, K. Mahdavi, *Appl. Surf. Sci.* **2019**, *463*, 283.
[74] A. Bhati, S. R. Anand, G. Gunture, A. K. Garg, P. Khare, S. K. Sonkar, *ACS Sustainable Chem. Eng.* **2018**, *6*, 9246.
[75] A. Ibarbia, H. J. Grande, V. Ruiz, *Part. Part. Syst. Charact.* **2020**, *37*, 2000061.
[76] M. Roushani, M. Mavaei, H. R. Rajabi, *J. Mol. Catal., A* **2015**, *409*, 102.
[77] J. Fan, D. Li, X. Wang, *Diamond Relat. Mater.* **2016**, *69*, 81.
[78] S. Kumar, A. K. Ojha, B. Ahmed, A. Kumar, J. Das, A. Materny, *Mater. Today Commun.* **2017**, *11*, 76.
[79] B. Ahmed, S. Kumar, A. K. Ojha, F. Hirsch, S. Riese, I. Fischer, *J. Photochem. Photobiol., A* **2018**, *364*, 671.
[80] B. N. Jusuf, N. S. Sambudi, I. Isnaeni, S. Samsuri, *J. Environ. Chem. Eng.* **2018**, *6*, 7426.
[81] G. S. Das, J. P. Shim, A. Bhatnagar, K. M. Tripathi, T. Y. Kim, *Sci. Rep.* **2019**, *9*, 1.
[82] P. Mandal, K. K. Nath, M. Saha, *Biointerface Res. Appl. Chem.* **2021**, *11*, 8171.
[83] H. Li, R. Liu, Y. Liu, H. Huang, H. Yu, H. Ming, S. Lian, S. T. Lee, Z. Kang, *J. Mater. Chem.* **2012**, *22*, 17470.
[84] H. Tian, K. Shen, X. Hu, L. Qiao, W. Zheng, *J. Alloys Compd.* **2017**, *691*, 369.
[85] S. Khan, A. K. Narula, *J. Mater. Sci.: Mater. Electron.* **2018**, *29*, 6337.
[86] K. H. Leong, S. Yang Fong, P. Feng Lim, L. Ching Sim, P. Saravanan, *IOP Conf. Ser. Mater. Sci. Eng.* **2018**, 409, 012009.
[87] H. Karimi, H. R. Rajabi, L. Kavoshi, *J. Photochem. Photobiol., A* **2020**, *397*, 112534.
[88] S. Asadzadeh-Khaneghah, A. Habibi-Yangjeh, D. Seifzadeh, H. Chand, V. Krishnan, *Colloids Surf., A* **2021**, *617*, 126424.
[89] S. Asadzadeh-Khaneghah, A. Habibi-Yangjeh, *J. Cleaner Prod.* **2020**, *276*, 124319.
[90] M. Shekofteh-Gohari, A. Habibi-Yangjeh, M. Abitorabi, A. Rouhi, *Crit. Rev. Environ. Sci. Technol.* **2018**, *48*, 806.
[91] A. Habibi-Yangjeh, S. Asadzadeh-Khaneghah, S. Feizpoor, A. Rouhi, *J. Colloid Interface Sci.* **2020**, *580*, 503.
[92] G. Sharma, S. Bhogal, M. Naushad, Inamuddin, A. Kumar, F. J. Stadler, *J. Photochem. Photobiol., A* **2017**, *347*, 235.
[93] J. Di, J. Xia, Y. Ge, H. Li, H. Ji, H. Xu, Q. Zhang, H. Li, M. Li, *Appl. Catal., B* **2015**, *168–169*, 51.
[94] F. Ming, J. Hong, X. Xu, Z. Wang, *RSC Adv.* **2016**, *6*, 31551.
[95] J. Liu, H. Xu, Y. Xu, Y. Song, J. Lian, Y. Zhao, L. Wang, L. Huang, H. Ji, H. Li, *Appl. Catal., B* **2017**, *207*, 429.
[96] S. Sharma, A. Umar, S. K. Mehta, A. O. Ibhadon, S. K. Kansal, *New J. Chem.* **2018**, *42*, 7445.
[97] P. Huo, J. Guan, M. Zhou, C. Ma, X. Liu, Y. Yan, S. Yuan, *J. Ind. Eng. Chem.* **2017**, *50*, 147.
[98] J. Di, J. Xia, X. Chen, M. Ji, S. Yin, Q. Zhang, H. Li, *Carbon* **2017**, *114*, 601.
[99] R. Jiang, G. Lu, Z. Yan, D. Wu, R. Zhou, X. Bao, *Chem. Eng. J.* **2019**, *374*, 79.
[100] M. Zhu, Q. Liu, W. Chen, Y. Yin, L. Ge, H. Li, K. Wang, *ACS Appl. Mater. Interfaces* **2017**, *9*, 38832.
[101] W. Zhu, X. Li, *Appl. Phys. A: Mater. Sci. Process.* **2017**, *123*, 272
[102] M. Ji, Z. Zhang, J. Xia, J. Di, Y. Liu, R. Chen, S. Yin, S. Zhang, H. Li, *Chin. Chem. Lett.* **2018**, *29*, 805.
[103] Z. Liang, J. Yang, C. Zhou, Q. Mo, Y. Zhang, *Inorg. Chem. Commun.* **2018**, *90*, 97.
[104] J. Zhang, M. Yan, X. Yuan, M. Si, L. Jiang, Z. Wu, H. Wang, G. Zeng, *J. Colloid Interface Sci.* **2018**, *529*, 11.
[105] J. Jiang, W. Shi, F. Guo, S. Yuan, *Inorg. Chem. Front.* **2018**, *5*, 1438.
[106] S. Sharma, S. K. Mehta, A. O. Ibhadon, S. K. Kansal, *J. Colloid Interface Sci.* **2019**, *533*, 227.
[107] Y. Sheng, D. Yi, H. Qingsong, W. Ting, L. Ming, C. Yong, S. Yifan, D. Jun, W. Bin, J. Xia, L. Huaming, *J. Photochem. Photobiol., A* **2019**, *382*, 111921.
[108] R. Jiang, D. Wu, G. Lu, Z. Yan, J. Liu, *Chemosphere* **2019**, *227*, 82.
[109] S. Le, W. Li, Y. Wang, X. Jiang, X. Yang, X. Wang, *J. Hazard. Mater.* **2019**, *376*, 1.
[110] J. Zhao, Q. He, X. Zhang, X. Guo, Q. Song, Y. Liu, B. Yao, Q. Zhang, D. D. Dionysiou, *Catal. Today* **2020**, *355*, 716.
[111] X. Tang, Y. Yu, C. Ma, G. Zhou, X. Liu, M. Song, Z. Lu, L. Liu, *New J. Chem.* **2019**, *43*, 18860.
[112] W. Liu, Y. Li, F. Liu, W. Jiang, D. Zhang, J. Liang, *Water Res.* **2019**, *150*, 431.
[113] X. Lin, C. Liu, J. Wang, S. Yang, J. Shi, Y. Hong, *Sep. Purif. Technol.* **2019**, *226*, 117.
[114] Y. Zhang, H. Pan, F. Zhang, *Mater. Lett.* **2019**, *251*, 114.
[115] Q. Chen, L. Chen, J. Qi, Y. Tong, Y. Lv, C. Xu, J. Ni, W. Liu, *Chin. Chem. Lett.* **2019**, *30*, 1214.
[116] W. Wang, Z. Zeng, G. Zeng, C. Zhang, R. Xiao, C. Zhou, W. Xiong, Y. Yang, L. Lei, Y. Liu, D. Huang, M. Cheng, Y. Yang, Y. Fu, H. Luo, Y. Zhou, *Chem. Eng. J.* **2019**, *378*, 122132.
[117] F. Guo, X. Huang, Z. Chen, H. Sun, W. Shi, *Sep. Purif. Technol.* **2020**, *253*, 117518.
[118] A. Kumar, A. Kumari, G. Sharma, B. Du, M. Naushad, F. J. Stadler, *J. Mol. Liq.* **2020**, *300*, 112356.
[119] Q. Liu, L. Zhou, J. Gao, S. Wang, L. Liu, S. Liu, *J. Colloid Interface Sci.* **2020**, *569*, 12.
[120] H. Yu, J. Huang, L. Jiang, Y. Shi, K. Yi, W. Zhang, J. Zhang, H. Chen, X. Yuan, *Chem. Eng. J.* **2020**, *402*, 126187.
[121] Y. Qu, X. Xu, R. Huang, W. Qi, R. Su, Z. He, *Chem. Eng. J.* **2020**, *382*, 123016.
[122] S. Le, W. Yang, G. Chen, A. Yan, X. Wang, *Environ. Pollut.* **2020**, *263*, 114550.
[123] Z. dong Lei, J. jun Wang, L. Wang, X. yu Yang, G. Xu, L. Tang, *J. Hazard. Mater.* **2016**, *312*, 298.
[124] D. Huang, L. Yin, X. Lu, S. Lin, Z. Niu, J. Niu, *Chem. Eng. J.* **2017**, *323*, 406.
[125] H. Lee, H. Anwer, J. W. Park, *Chemosphere* **2020**, *246*, 125761.
[126] R. Hatefi, A. Mashinchian-Moradi, H. Younesi, S. Nojavan, *J. Environ. Health Sci. Eng.* **2020**, *18*, 1531.
[127] A. Bhati, S. R. Anand, D. Saini, Gunture, S. K. Sonkar, *npj Clean Water* **2019**, *2*, 12.
[128] Y. Zhang, Y. Zhao, Z. Xu, H. Su, X. Bian, S. Zhang, X. Dong, L. Zeng, T. Zeng, M. Feng, L. Li, V. K. Sharma, *Appl. Catal., B* **2020**, *262*, 118306.
[129] Y. Y. Liu, N. Y. Yu, W. Di Fang, Q. G. Tan, R. Ji, L. Y. Yang, S. Wei, X. W. Zhang, A. J. Miao, *Nat. Commun.* **2021**, *12*, 812.

Kamran Akbar received his Ph.D. at the Sejong University (South Korea) in 2018, working on the growth of vertical graphene nanohills for electrocatalysis applications, with Prof. Seung-Hyun Chun. Thereafter, he has joined the Department of Energy Science, Sungkyunkwan University (South Korea) as a postdoctoral researcher. His research interests include the development of 2D material quantum dots and Organo halide perovskites for applications in catalysis and memory devices. Currently, he is working with Prof. Alberto Vomiero and Prof. Elisa Moretti in Ca Foscari University of Venice (Italy) as senior postdoctoral fellow. His research activities include single atom catalysis, photo/electro-catalysis, and solar water evaporation.

Elisa Moretti is an associate professor in Inorganic Chemistry at the Department of Molecular Sciences and Nanosystems, Ca' Foscari University of Venice (Italy). After receiving a Ph.D. Degree in Chemistry (2005) at the Ca' Foscari University, she moved to the University of Malaga (Spain) for a postdoctoral experience in the group of Prof. E. Rodriguez-Castellon. Prof. Moretti's research interests focus on 0-3D nanostructured inorganic materials, mainly multicomponent oxide systems, for catalytic and photocatalytic applications (on board H2 purification by CO preferential thermal/photo-oxidation, dyes and drugs photodegradation for water remediation).

Alberto Vomiero is a chair professor of Experimental Physics at the Department of Engineering Sciences and Mathematics, Luleå University of Technology, Sweden and a professor of Industrial Engineering at the Department of Molecular Sciences and Nanosystems, Ca' Foscari University of Venice, Italy. He is leading a multidisciplinary group focusing on the development of advanced nanomaterials for energy and environmental applications, including solar cells, water splitting, and photocatalysis. He is a former Marie Curie International Outgoing Fellow of the European Commission, Fellow of the Swedish Foundations, of the Royal Society of Chemistry, and several other Societies.